

2. EXPLANATORY NOTES¹

Shipboard Scientific Party²

INTRODUCTION

This chapter is designed to document the primary procedures and methods employed by the various shipboard laboratories as a basis for understanding the preliminary interpretations in this volume. This information concerns only shipboard methods described in the site reports in the Leg 191 *Initial Reports* volume of *Proceedings of the Ocean Drilling Program* (ODP).

SHIPBOARD SCIENTIFIC PROCEDURES

Numbering of Sites, Holes, Cores, and Samples

Drilling sites are numbered consecutively from the first site drilled by the *Glomar Challenger* in 1968. A site refers to one or more holes drilled while the ship was positioned over one acoustic beacon. At a site, multiple holes can be drilled by removing the drill pipe from the seafloor, moving the ship a short distance, and then drilling a new hole. For all ODP drill sites, a letter suffix distinguishes each hole drilled at the same site. The first hole drilled is assigned the site number modified by the suffix "A," the second hole takes the site number and suffix "B," and so forth.

The cored interval is measured in meters below seafloor (mbsf). The depth below seafloor is determined by subtracting the water depth estimated from the initial drill pipe measurement, which gives the length of pipe from the rig floor to the seafloor (measured in meters below rig floor, mbrf), from the total drill pipe measurement. Each cored interval is generally 9.5 m long, which is the length of a core barrel. Cored intervals may be shorter and may not necessarily be adjacent if separated by drilled intervals.

¹Examples of how to reference the whole or part of this volume.

²Shipboard Scientific Party addresses.

A recovered core is divided into 1.5-m sections that are numbered serially from the top. When full recovery is obtained, the sections are numbered from one through seven, with the last section possibly being shorter than 1.5 m (Fig. F1); rarely, an unusually long core may require more than seven sections. When less than full recovery is obtained, there will be as many sections as needed to accommodate the length of the core recovered. By convention, material recovered from the core catcher of a sediment core is placed in a separate section during the core description, labeled core catcher (CC), and placed below the last section recovered in the liner. The core catcher is placed at the top of the cored interval in cases where material is only recovered in the core catcher.

When the recovered core is shorter than the cored interval, the top of the core is equated with the top of the cored interval by convention to achieve consistency in handling analytical data derived from the cores. Samples removed from the cores are designated by distance measured in centimeters from the top of the section to the top and bottom of each sample removed from that section. A full identification number for a sample consists of the following information: leg, site, hole, core number, core type, section number, piece number (for hard rock), and interval in centimeters measured from the top of section. For example, a sample identification of “191-1179C-3H-5, 80–85 cm” would be interpreted as representing a sample removed from the interval between 80 and 85 cm below the top of Section 5, Core 3 (H designates that this core was taken during hydraulic piston coring) of Hole 1179C from Leg 191 (Fig. F1).

All ODP core identifiers indicate core type. The following abbreviations are used:

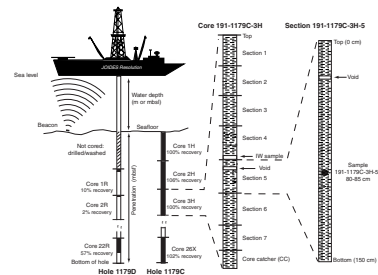
- H = hydraulic piston corer (also referred to as APC, or advanced hydraulic piston corer).
- X = extended core barrel (XCB).
- R = rotary core barrel (RCB).
- M = miscellaneous material.

CORE HANDLING

Sediments

As soon as a core is retrieved on deck, a sample is taken from the core catcher and given to the paleontological laboratory for an initial age assessment. Then the core is placed on a long horizontal rack, and gas samples may be taken by piercing the core liner and withdrawing gas into a vacuum tube. Voids within the core are sought as sites for gas sampling. Some of the gas samples are stored for shore-based study; however, others are analyzed immediately as part of the shipboard safety and pollution-prevention program. Next, the core is marked into section lengths, each section is labeled, and the core is cut into sections. Headspace gas samples are scraped from the ends of cut sections on the catwalk and sealed in glass vials for light hydrocarbon analysis. Each section is then sealed at the top and bottom by gluing on color-coded plastic caps, blue to identify the top of a section and clear to identify the bottom. A yellow cap is placed on the section ends from which a whole-round sample has been removed. The caps are usually attached to the liner by coating the end liner and the inside rim of the cap with acetone, and then the caps are taped to the liners. Additionally, during

F1. Illustration of hole, core, section, and sample numbering, p. 38.



Leg 191, sediment samples were taken on the deck for microbiology studies. Special handling of these samples is specified in "[Microbiology and Inorganic Geochemistry](#)," p. 14.

Next, the cores are carried into the laboratory, where the sections are labeled again, using an engraver to mark the full designation of the section permanently on the core liner. The length of the core in each section and the core-catcher sample are measured to the nearest centimeter; this information is logged into the shipboard CORELOG database program. After cores have equilibrated to room temperature (~3 hr), they are run through the multisensor track (MST), thermal conductivity measurements are performed on relatively soft sediments, and the cores are split.

Cores of soft material are split lengthwise into working and archive halves. The softer cores are split with a wire or saw, depending on the degree of induration. Harder cores are split with a band saw or diamond saw. During Leg 191, the wire-cut cores were split from the bottom to top; thus, investigators should be aware that older material may have been transported up the core on the split face of each section.

The working half of the core is sampled for both shipboard and shore-based laboratory studies. Each extracted sample is logged into the sampling computer database program by the location and the name of the investigator receiving the sample. Records of all removed samples are kept by the curator at ODP. The extracted samples are sealed in plastic vials or bags and labeled. Samples are routinely taken for shipboard physical properties analysis, magnetic studies, and for calcium carbonate (coulometric analysis) and organic carbon (CNS elemental analyzer) analyses.

The archive half is described visually (see "[Sediment Description](#)," p. 5). Smear slides are made from sediment samples taken from the archive half. Most archive sections are run through the archive multisensor track (AMST), for magnetic susceptibility and color reflectance spectroscopy measurements, and the cryogenic magnetometer. The archive half then is photographed using black-and-white and color film. Close-up photographs (color and black and white) are taken of particular features for illustrations in the summary of each site, as requested by individual scientists.

Both halves of the core then are placed into labeled plastic tubes, sealed, and transferred to cold-storage space aboard the drilling vessel. At the end of the leg, the cores are transferred from the ship in refrigerated airfreight containers to cold storage at ODP's Gulf Coast Repository at Texas A&M University.

Igneous and Metamorphic Rocks

Igneous rock cores are handled differently from sediment cores. Once on deck, the core-catcher sample is placed at the bottom of the core liner and total core recovery is calculated by pushing the rock pieces together and measuring to the nearest centimeter. This information is logged into the shipboard CORELOG database program. The core then is cut into 1.5-m-long sections and transferred into the laboratory.

The contents of each section are transferred into 1.5-m-long sections of split core liner, where the bottom of oriented pieces (i.e., pieces that clearly could not have rotated top to bottom about a horizontal axis in the liner) are marked with a red wax pencil. This is done to ensure that orientation is not lost during the splitting and labeling processes. Important primary features of the cores also are recorded at this time. The

core then is split into archive and working halves. A plastic spacer is used to separate individual pieces and/or reconstructed groups of pieces in the core liner. These spacers may represent a substantial interval of no recovery. Each piece is numbered sequentially from the top of each section, beginning with number 1; reconstructed groups of pieces are assigned the same number but are lettered consecutively. Pieces are labeled only on the outer cylindrical surfaces of the core. If the piece is oriented, an arrow is added to the label pointing to the top of the section. Because pieces are free to turn about a vertical axis during drilling, determination of azimuthal orientation during Leg 191 was possible only by using paleomagnetic or downhole logging data.

In splitting the core, every effort is made to ensure that important features are represented in both halves. The working half is sampled for shipboard physical properties measurements, magnetic studies, X-ray fluorescence (XRF), X-ray diffraction (XRD), and thin-section studies. Nondestructive physical properties measurements, such as magnetic susceptibility, are performed on the archive half of the core. Where recovery permits, samples are taken from each lithostratigraphic unit. Some of these samples are minicores. Records of all samples are kept by the curator at ODP. The archive half then is photographed using black-and-white and color film. Close-up photographs (color and black and white) are taken of particular features for illustrations in the summary of each site, as requested by individual scientists. Both halves of the core then are shrink-wrapped in plastic to prevent rock pieces from vibrating out of sequence during transit, placed into labeled plastic tubes, sealed, and transferred to cold-storage space aboard the drilling vessel. As with the other Leg 191 cores, they are housed at ODP's Gulf Coast Repository at Texas A&M University.

SITE GEOPHYSICS

Drilling during Leg 191 occurred at four sites, the last three characterized only by underway profile data collected by the *JOIDES Resolution* owing to extraordinary circumstances. The International Ocean Network seismometer hole at Site 1179 (proposed Site WP-2A) was sited on data collected in 1996 by the *Hakuho-Maru* (Ocean Research Institute, University of Tokyo) during cruise KH96-3 (Leg 1). Hammer-drill tests, originally scheduled for a site on Shatsky Rise, were moved to two seamounts near Guam after problems with the drilling equipment dictated picking up spare parts in Guam. No geophysical data were on board for these hammer-drill test sites, but because the goal was to find a basalt outcrop near a seamount summit, it was sufficient to survey for possible sites with the *Resolution's* echo sounders. No single-channel seismic (SCS) data were collected during Leg 191 because it was not deemed necessary. The main site (1179) was characterized by multichannel seismic lines navigated by Global Positioning System (GPS), so it was possible to precisely locate the desired drilling location without resurveying. Furthermore, the hammer-drill test sites are on the tops of young seamounts where SCS data would have provided little useful information.

Underway geophysical data collected during all Leg 191 transits and surveys were 3.5-kHz and 12-kHz echo-sounder profiles and total field magnetic data collected with a proton precession magnetometer.

Navigation

GPS positioning was used throughout Leg 191. Three GPS systems were available for operation, with output provided to the underway geophysics laboratory. An Ashtech GG24 receiver was used as the primary navigation device throughout the leg. Older Omnistar and Magnavox GPS systems were available but not used.

GPS fixes were available continuously (1-s updates) and were recorded at 60-s intervals. Event data were recorded at 60-s intervals on site and in transit. Navigation data were logged by the WINFROG software system, mounted on a dedicated PC in the underway geophysics laboratory. Subsequent processing and display of navigation data were performed using the Generic Mapping Tools software package (Wessel and Smith, 1995) on shipboard UNIX workstations.

Echo Sounder

Two echo sounders (precision depth recorders) were used during transits: 3.5-kHz and 12-kHz frequency units. The former was used to acquire bathymetric data as well as high-resolution reflection records of the uppermost sediment layers. Data from both systems were recorded on EPC 8082 analog line-scanning recorders. The 3.5-kHz system used a Raytheon CESP III correlator echo-sounder processor driven by a Raytheon PTR105B transceiver with a 2-kW sonar transmitter and included a single EDO type-323c transducer mounted in a sonar dome on the hull 40 m forward of the center of the moonpool. This location was chosen to reduce ship-generated noise and signal attenuation from aeration beneath the hull. The recorder was annotated automatically at fixed intervals; ship speed and heading were marked every 5 min and position every 30 min. Depth readings were taken manually every 5 min and entered into an Excel spreadsheet.

Magnetometer

Total intensity measurements of the Earth's magnetic field were obtained with a Geometrics Model G-886 proton precession magnetometer towed ~500 m astern. Magnetic data were recorded during transits at 1-min intervals on navigation files produced by WINFROG navigation software.

SEDIMENT DESCRIPTION

The description of sedimentary units recovered during Leg 191 included estimates of sediment composition based on smear slides, thin sections, carbonate and XRD measurements, and documentation of sedimentary and deformational structures, drilling disturbance, presence and type of fossils, bioturbation intensity, induration, diagenetic alteration, and color. These data were recorded manually for each core section on standard Visual Core Description (VCD) paper forms that are archived by ODP. This section is chiefly a reproduction of the "Sediment Description" section in the "Explanatory Notes" chapter of the Leg 185 *Initial Reports* volume (Shipboard Scientific Party, 2000), with modifications reflecting the pelagic lithologies encountered during Leg 191.

Barrel Sheet Data

Information on the VCDs was summarized and entered into AppleCORE (version 8.1f) software, which generates a one-page graphical log of each core (barrel sheet). Barrel sheets are presented with core photographs in the “[Core Descriptions](#)” contents list. A wide variety of features, such as sediment lithology, bed thickness, primary sedimentary structures, bioturbation parameters, soft-sediment deformation, and structural and diagenetic features are indicated by patterns and symbols in the graphic logs. A key to the full set of patterns and symbols used on the barrel sheets is shown in Figure F2. The symbols are schematic but are placed as close as possible to their proper stratigraphic position or arrows indicate the interval to which the symbol applies. For exact positions of sedimentary features, copies of the detailed section-by-section VCD forms can be obtained from ODP. Barrel sheets consist of the following columns, each of which is discussed in detail below: lithology, texture and structure, sedimentary structures, bioturbation, drilling disturbance, samples, color, and description.

Lithology

Sediment lithologies are represented by patterns in the Lithology column (see the “[Core Descriptions](#)” contents list for examples). This column may consist of up to three vertical strips depending on the number of the major end-member constituents (see “[Sediment Classification](#),” p. 10), thus reflecting intermixing of different components. Sediments with only one major component group (i.e., all other component groups being below 10% each) are represented by one strip. Because of the limitations of the AppleCORE software, thin intervals of interbedded lithologies cannot be adequately displayed at the scale used for the barrel sheets but they are described in the Description column of the barrel sheets, where appropriate.

Texture and Structure

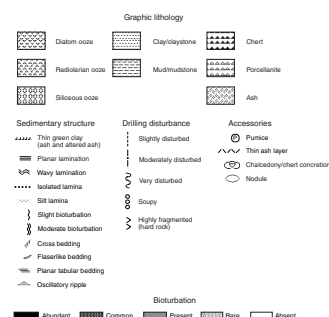
With exceptions as noted below, the terms and parameters for texture and sedimentary structure that are used for this leg are compatible to those mentioned in the handbooks of Mazzullo and Graham (1988) or Folk (1980). Sediments were examined in terms of texture, including grain size, shape, sorting, and fabric, with the aid of hand lenses, smear slides, and thin sections. See, however, the comments below on the near-worthlessness of mandated grain-size estimates taken from smear slides, especially in reference to pelagic oozes. Primary and secondary sedimentary structures were described from observations of the split surface of the archive cores.

Sedimentary Structures

Symbols for bioturbation, structures, accessories, and drilling disturbances are shown in Figure F2.

The bulk of the pelagic sediments recovered during Leg 191 were relatively homogeneous. Stratification, bioturbation, or other sedimentary structures were usually only discernible where textural or compositional differences were present (e.g., close to ash layers). In the homogeneous background sediment, however, it was difficult to distinguish the destruction of primary structures by bioturbation from the actual ab-

F2. Key to symbols used in the barrel sheets, p. 39.



sence of primary structures. Given the light gray and reddish colors of the siliceous and clayey sediments, the absence of lamination, and the very low organic matter contents, it is reasonable to assume that the remaining sediment has been pervasively bioturbated as well because benthic burrowing activity was not limited by oxygen deficiency. To convey the maximum amount of information without confusing interpretation with observation, we used the Bioturbation column to display only visible bioturbation or sediment mottling. The Bioturbation column of the barrel sheets shows four levels of intensity as follows:

Homogeneous = trace fossils are either absent or invisible because they occur in a completely biogenic fabric.
Low = rare, discrete burrows.
Moderate = burrows are generally isolated but locally overlap.
Intense = abundant, overlapping burrows. Several generations of bioturbation structures cut across each other resulting in almost total disruption of sedimentary structures.

Stratification thickness was characterized using a combination of the terms given by McKee and Weir (1953) and Ingram (1954):

Very thick bedded = >1 m thick.
Thick bedded = 30–100 cm thick.
Medium bedded = 10–30 cm thick.
Thin bedded = 3–10 cm thick.
Very thin bedded = 1–3 cm thick.
Thickly laminated = 3–10 mm thick.
Thinly laminated = 1–3 mm thick.
Very thinly laminated = <1 mm thick.

Drilling Disturbance

Natural structures (physical or biological) can be difficult to distinguish from disturbance created by the coring process. Deformation and disturbance of sediment that resulted from the coring process are illustrated in the Drilling Disturbance column, using symbols shown in Figure F2. Blank regions indicate the absence of drilling disturbance. The degree of drilling disturbance for soft sediments was described using the following categories:

Slightly disturbed = bedding contacts slightly bent.
Moderately disturbed = bedding contacts bowed.
Highly disturbed = bedding hardly discernible, commonly showing flow structures.

There are standard ODP categories for describing fragmentation in indurated sediments and rock, but the only one appropriate for Leg 191 was the following, for the cherty interval:

Highly fragmented = core pieces are from the interval cored and are probably in correct stratigraphic sequence (although they may not represent the entire section), but the original orientation is completely lost.

Samples and Close-Up Photographs

The stratigraphic position of samples taken for shipboard analysis is indicated in the Samples column of the barrel sheet according to the following codes:

PAL = biostratigraphy.
SS = smear slide.
TS = thin section.
WH = whole-core sample.
XRD = X-ray diffraction.

Color

Sediment color was determined visually by comparison with standard color charts (Munsell Color Company, Inc., 1975; Rock Color Chart Committee, 1991) and is reported in the VCD Color column and the Description column of the barrel sheets. In addition to determining color visually, all cores were scanned at 2- to 5-cm intervals using a Minolta CM-2002 spectrophotometer mounted on the AMST. The spectrophotometer measures reflectance in thirty-one 10-nm-wide bands of the visible spectrum (400–700 nm) on the archive half of each core section. Spectrophotometer readings were taken after cleaning the surface of each core section and covering it with clear plastic film (Glad Cling Wrap). Calibration of the color scanner did not include a correction for the plastic film because we found the effect to be very minor even with very brightly colored lithologies. The measurements were taken automatically and recorded by the AMST at evenly spaced intervals along each section. There was no way to program the AMST software to avoid taking measurements in intervals with a depressed core surface or in disturbed areas of core with drilling slurry or biscuits. The data are part of the Janus database and can be obtained from ODP (see the “[Related Leg Data](#)” contents list). Additional detailed information about measurement and interpretation of Minolta spectrophotometer spectral data can be found in Balsam et al. (1997, 1998, 2000).

Description

A summary of the lithologic observations is given in the Description column of the barrel sheets. It consists of three parts: (1) a heading in capital letters that lists only the dominant sediment lithologies observed in the core; (2) a general description of the core, including color, composition, sedimentary structures, bed thicknesses, drilling disturbance, as well as any other general features in the core; and (3) descriptions and locations of thin, interbedded, or minor lithologies.

Smear Slides and Thin Sections

Sediments were analyzed petrographically using smear slides and thin sections. Tables summarizing these data (see the “[Core Descriptions](#)” contents list) include information about the sample location, whether the sample represents a dominant (D) or a minor (M) lithology in the core, and an estimate of the percentages of sand-, silt-, and clay-sized fractions, together with all identified components. We emphasize here that smear-slide and thin-section analyses provide only estimates of the relative abundances of the constituents. The comparison charts

of Baccelle and Bossellini (1965, in Flügel, 1982) were used to refine abundance estimates in thin sections. However, these charts cannot be used for smear slides because they are designed to simulate a field of view that is completely and evenly covered with particles. Quantification of data from smear slides is further complicated by the difficulty of identifying fine-grained particles using only a microscope and by the tendency to underestimate sand-sized grains because they cannot be incorporated evenly into the smear. Biogenic opal and its diagenetic modifications are particularly difficult to determine from smear slides (van Andel, 1983). Previous experience has shown that the largest variations in smear-slide determination correlate with the change from one observer to another or with shift changes. The accuracy problem is indicated in the "Explanatory Notes" chapters of several recent ODP *Initial Reports* volumes in which sedimentologic numerical data in general, and those of smear-slide determination in particular, are consistently deemphasized and replaced by semiquantitative categories (e.g., Shipboard Scientific Party, 1998a, 1998b, 1998c, 2000). A limitation to semiquantitative categories, such as the ones proposed during previous legs, would have seemed all the more appropriate during Leg 191. Current ODP policies, however, require the input of numerical data, and so the reader is warned that the tabulated smear-slide results (see the "[Core Descriptions](#)" contents list) largely reflect the need to comply with these regulations rather than actual accuracy. Smear-slide and thin-section data were reviewed for internal consistency and correct sedimentologic nomenclature, and the qualitative composition was confirmed by XRD. Accuracy of the carbonate content estimated from smear slides and thin sections was confirmed by chemical analyses.

X-Ray Diffraction Analysis

Selected samples were taken for qualitative mineral analysis by XRD using a Philips diffractometer with CuK_α radiation at 40 kV and 35 mA with a focusing graphite monochromator and the following slit settings:

Focus	= fine.
Irradiated length	= 12 mm.
Divergence slit	= automatic.
Receiving slit	= 0.2 mm.
Step size	= $0.02^\circ 2\theta$.
Count time per step	= 1 s.
Scanning rate	= $2^\circ 2\theta/\text{min}$.
Ratemeter time constant	= 0.2 s.
Spinner	= off.
Monochromator	= on.
Scan	= continuous.

Bulk samples were freeze-dried, ground using an agate mortar and pestle, and packed in sample holders, which, together with the ship's movement, probably imparted some orientation to the mineral powder. These samples were scanned from 2° – $70^\circ 2\theta$. MacDiff software (v. 4.0.4 PPC, by Rainer Petschick) was used to display diffractograms and to identify the minerals. Most diffractograms were corrected to match the main peaks of quartz, calcite, or clinoptilolite at 3.343, 3.035, and 8.95 Å, respectively. Identifications are based on multiple peak matches using the

mineral database provided with MacDiff. Relative abundances reported in this volume are useful for general characterization of the sediments, but they are not quantitative concentration data.

Sediment Classification

We evaluated the methods and the classification used for sediment description and found that there is a need for a less ambiguous and more flexible classification than the proposed ODP standard classification by Mazzullo et al. (1988). Our classification is neither comprehensive nor entirely descriptive, but it is simple to use for the purpose of Leg 191 and it circumvents some of the disadvantages of the Mazzullo classification. Notably, it avoids the impression of a level of accuracy that is not achievable under the conditions of most ODP cruises. Also, we tried to use common and relatively simple names, which led us to abandon a number of terms. For the deep pelagic Site 1179, we used the three end-members, diatoms, radiolarians, and clay (Fig. F3), that represent virtually all of the section (except for some ashy and zeolitic intervals) that lies above the cherts.

Sediment Nomenclature

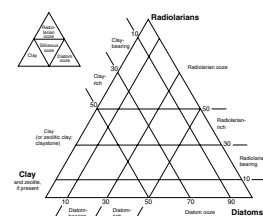
Sediment names at Site 1179 consist of one of four principal names relating to the dominant composition of the sediment (e.g., clay, diatom ooze, and radiolarian ooze, where any one of those three is more abundant than 50%) and siliceous ooze (if neither diatoms nor radiolarians is more than 50% but together they are) and of modifiers that precede the principal name. A component with 10%–30% abundance is termed component bearing, and one with 30%–50% is termed component rich (e.g., ash-bearing clay and radiolarian-rich diatom ooze).

Sedimentary rock is named according to composition and induration. Except for some thin zeolitic layers firm enough to be called mudstone or claystone, sedimentary rock recovered is termed porcellanite if it is firm to hard and chert if it is hard enough to resist scratching by a stainless steel probe. Porcellanite is dull in appearance and is commonly less dense than vitreous to waxy dense chert. In addition to this field classification, the terms porcellanite and chert bear a strong compositional notion. Thus, porcellanite is typically composed of opal-CT (cristobalite-trydimite) but may also contain diagenetic quartz, carbonate, and silicates (mostly clay minerals). Chert is usually dominated by quartz and tends to be purer silica but may also contain clay minerals and carbonate (Isaacs, 1982; Isaacs et al., 1983). The hard lithologies we recovered were almost entirely pieces of chert.

Siliciclastic, Volcaniclastic, and Authigenic Silicate Sediment

No lithology had sufficient detrital sand or silt to earn it a sediment name. Detrital components, however, include fine sand- through silt-sized grains of quartz and feldspar of eolian origin. A few grains of hornblende and pyroxene were found. Sand grain size is between 2 mm and 63 μm , silt is between 63 and 2 μm , and clay is material finer than 2 μm . Where they do not compose ooze, mixtures of sand, silt, and clay texture are named according to the classification of Folk (1980) and for a few thin layers the suffix *-stone* is added if the sediment is indurated. Note that the silt-to-clay boundary has been placed at 2 μm , as sug-

F3. Sediment classification nomenclature and schematic, p. 40.



gested by Doeglas (1968). The principal name for sediments dominated by volcanoclastic components in the silt- and fine sand-size range (250–2 μm) is volcanic ash. No ash was sufficiently indurated to earn the name tuff, and no hyaloclastite was observed, except that interlayered with basalt crust.

Clay that is present in almost all cores probably is partly eolian, partly far traveled in suspension, and partly authigenic. The grain size of zeolite that is present in many cores seems to depend largely on the vigor of the smear-slide preparation, and so in the classification, clay and zeolite are commonly lumped as zeolitic clay.

BIOSTRATIGRAPHY

Introduction

During Leg 191, calcareous nannofossils, foraminifers, palynomorphs, and radiolarians were studied in order to assess biostratigraphic constraints on the sedimentary section at Site 1179. The reference time scale adopted for Leg 191 follows Gradstein et al. (1994, 1995) for the Cretaceous and Berggren et al. (1995a) for the Cenozoic. Specific biozonations for each fossil group are discussed below in more detail.

Calcareous Nannofossils

We referred primarily to the zonations of Okada and Bukry (1980) and Martini (1971) for Cenozoic sediments and Perch-Nielsen (1983) for Cretaceous sediments. To facilitate comparison with other studies, numerical ages used are those compiled by Berggren et al. (1995a). Calcareous nannofossil assemblages were described from smear slides prepared for each core-catcher sample and for as many additional core samples as time permitted. Standard preparation techniques were used throughout. Examination was performed exclusively with a light microscope, using whatever optical configuration yielded useful results. In all cases, a magnification of 1000 \times was used to make semiquantitative estimates of abundances. Abundances of individual species were estimated for each sample. Five levels of individual species abundance were recorded, with the following approximate definitions:

- R = rare (1 specimen per 51 or more fields of view).
- F = few (1 specimen per 11–50 fields of view).
- C = common (1 specimen per 2–10 fields of view).
- A = abundant (1–10 specimens per field of view).
- V = very abundant (>10 specimens per field of view).

Total abundance of calcareous nannofossils for each sample was estimated as follows:

- B = barren (none).
- R = rare (1–10 specimens per 500 fields of view, about three traverses).
- F = few (11–50 specimens per 500 fields of view).
- C = common (51–2000 specimens per 500 fields of view).
- A = abundant (2001–20,000 specimens per 500 fields of view).
- V = very abundant (>20,000 specimens per 500 fields of view).

The qualitative evaluation of the preservation of calcareous nannofossils was recorded as poor, moderate, or good. These categories represent subjective impressions according to the following definitions:

- P = poor. Severe dissolution, fragmentation, and/or overgrowth has occurred. Primary features may have been destroyed, and many specimens cannot be identified to the species level.
- M = moderate. Dissolution and/or overgrowth are evident. A significant proportion (up to 10%) of the specimens cannot be identified to species level with absolute certainty.
- G = good. There is little or no evidence of dissolution and/or overgrowth. Diagnostic characteristics are preserved, and nearly all specimens can be identified to species level.

Dinoflagellate Cysts

No widely accepted dinocyst zonation exists for the Neogene to Holocene, but ages for these sediments are based mainly on the dinocyst biozonations of Powell (1992) and Harland (1992), which are derived largely from western Europe. The work of Matsuoka (1983) on late Cenozoic dinoflagellates and acritarchs in central Japan proved to be extremely useful at this western North Pacific site. Our Pleistocene biostratigraphy is supplemented by the zonation developed for the midlatitude North Atlantic by McCarthy et al. (2000). The Northern Hemisphere composite range estimates for Mesozoic–Cenozoic strata of Williams et al. (1993) and dinocyst datums established in various Deep Sea Drilling Project (DSDP) and ODP holes (e.g., de Verteuil, 1996; McCarthy and Mudie, 1996; Mudie, 1987) were also used to determine ages.

As many 20-cm³ core-catcher samples were examined as time permitted. Additional 20-cm³ samples were examined from intervals of particular stratigraphic interest. Processing consisted of heating the sample in a 1% Calgon solution until clays were disaggregated followed by sieving through a 10- μ m Nitex nylon sieve. Residues were then digested in hot 10% hydrochloric acid and washed with distilled water. Because of high silica content, samples were digested for ~1 hr in hot concentrated hydrofluoric acid and again washed with water. This was followed by a second sieving through a 10- μ m Nitex nylon sieve. Swirling the organic residues in a large watchglass removed residual coarse silicates, sulfides, and detrital minerals when they were present. Residues were strew mounted in glycerine jelly on glass slides and examined in bright field transmitted light at 250–400 \times magnification. Absolute abundances (or concentrations) of dinocysts and terrestrial palynomorphs (pollen and spores) were estimated and are reported as cysts per cubic centimeter of sediment. Samples were spiked with a tablet containing a known quantity of *Lycopodium clavatum* spores following the method of Stockmarr (1971) to determine absolute palynomorph concentrations. Relative species abundances are reported as follows:

- R = rare (<3%).
- F = few (3%–15%).
- C = common (15%–30%).
- A = abundant (>30%).

Qualitative evaluation of the preservation of dinocysts only is recorded as poor, moderate, or good. These categories represent subjective impressions with approximately the following meaning:

- P = poor. Severe bacterial infestation, chemical oxidation, and/or mechanical fragmentation have occurred. Primary features were destroyed, and many specimens cannot be identified to the species level.
- M = moderate. Bacterial infestation, chemical oxidation, and/or mechanical fragmentation are evident. Up to 25% of the specimens cannot be identified to species level with certainty.
- G = good. Little or no evidence exists of bacterial infestation, chemical oxidation, or mechanical fragmentation; essentially all (>95%) specimens can be identified to the species level.

All assemblages recovered are thermally immature, and therefore, thermal alteration is not a relevant factor in fragmentation or color alteration of palynomorphs.

Foraminifers

Samples of ~25 mL were soaked in a Calgon solution, washed through a 63- μ m sieve, and dried under a heat lamp.

Benthic and planktonic foraminifers were examined from the >150- μ m size fraction. Species abundance relative to the total foraminifer fauna was estimated as follows:

- B = barren (none).
- R = rare (<1%).
- F = few (1%–4%).
- C = common (5%–20%).
- A = abundant (>20%).

Preservation characteristics were divided into four categories:

- P = poor (almost all specimens were dissolved or broken and fragments dominated).
- M = moderate (30%–60% of specimens showed dissolved or broken chambers).
- G = good (60%–90% of specimens were well preserved and unbroken).
- VG = very good (>90% of specimens were well preserved and unbroken).

The foraminifers were used primarily as carbonate preservation indicators. For identification, Loeblich and Tappan (1988) was used.

Radiolarians

To obtain radiolarians from CC samples, ~10 cm³ of sediment was disaggregated and boiled using 10% H₂O₂, 10% HCl, and ~1% Calgon solutions. Brief treatment of samples in an ultrasonic bath was followed by washing on a 63- μ m mesh sieve. The residue was moved into a beaker, and a strewn slide was made using a pipette. Canada balsam was used as a mounting medium. Additional random strewn slides will be

prepared onshore to locate biostratigraphic events more accurately within cores. Overall radiolarian abundance was determined based on strewn-slide evaluation at 100× using the following conventions:

- B = barren (no radiolarians in sample).
- T = trace (<1 specimen per traverse).
- R = rare (1–10 specimens per traverse).
- F = few (11–50 specimens per traverse).
- C = common (51–100 specimens per traverse).
- A = abundant (>100 specimens per traverse).

The abundance of individual species was recorded relative to the fraction of the total assemblage as follows:

- B = barren (absent).
- T = trace (present in slide).
- R = rare (a few or more specimens per slide).
- F = few (<5% of the total assemblage).
- C = common (5%–10% of the total assemblage).
- A = abundant (>10% of the total assemblage).

Preservation was recorded as follows:

- P = poor (strong dissolution, recrystallization, or breakage; many specimens unidentifiable).
- M = moderate (minor but common dissolution with a small amount of recrystallization or breakage of specimens).
- G = good (majority of specimens complete with minor dissolution, recrystallization, and/or breakage).
- E = excellent (nearly pristine complete skeleton lacking any indication of dissolution, recrystallization, or breakage).

MICROBIOLOGY AND INORGANIC GEOCHEMISTRY

In response to organic matter deposition and the relative concentrations of dissolved oxygen, bacteria catalyze many redox reactions in sediments. These reactions influence the pore-water profiles of many compounds, such as nitrate, ammonia, phosphate, dissolved and particulate phases of manganese and iron, sulfate, and methane. Therefore, whereas pore-water chemistry is important for understanding sediment chemistry and diagenesis, pore-water chemistry profiles also reveal the habitats of many different types of aerobic and anaerobic bacteria (e.g., nitrifying and denitrifying bacteria, sulfate-reducing and sulfide-oxidizing bacteria, and methane-oxidizing and methanogenic bacteria).

The first core of Hole 1179B was designated specifically for microbiological and geochemical sampling at closer depth intervals near the sediment/water interface. In this core, samples were collected for sedimentary and pore-water analyses at the following depths: 0.1, 0.14, 0.25, 0.50, 0.75, 1, 4, 5, 6, and 7 mbsf. In subsequent cores, sediments and pore waters were collected from the following depths: 10, 20, 30, 40, 50, 60, 70, 80, 90, 100, 125, 150, 175, 200, 225, and 250 mbsf. All of these samples were collected with APC coring.

Interstitial Water Sampling and Chemical Analyses

Five- to ten-centimeter whole-round core (WRC) samples were collected for analysis of interstitial water (IW). Prior to squeezing the WRC for IW, ~3 cm³ of sediment was collected for carbonate and carbon, nitrogen, and sulfur (CNS) analyses. In addition, the squeeze cakes left over from pore-water collection were reserved for coulometric determination of carbonate, CNS analysis, and inductively coupled plasma-atomic emission spectroscopy (ICP-AES) analyses of Fe and Mn.

IWs were retrieved by applying the minimum pressure necessary to the sediment and gradually increasing it up to a maximum pressure of 205 MPa (30,000 psi) using a hydraulic press (Manheim and Sayles, 1974). Before squeezing, the sediment was immediately extruded from the whole-round core liner, the surface was carefully scraped to remove potentially contaminated exteriors, and the cleaned sediment was placed into a titanium squeezer atop a filter previously rinsed with high purity water to remove processing acids. Interstitial water was collected in two splits. An unfiltered sample was immediately treated with zinc acetate at 12.5 mg/10 mL of sample and frozen for subsequent shore-based $\delta^{34}\text{S}$ analysis of the sulfate. The other IW split used for routine chemical analyses was passed through a filter into a plastic syringe attached to the bottom of the squeezer assembly and filtered through a 0.45- μm polycarbonate filter. Samples were stored in plastic vials pending shipboard analyses. Archived aliquots for future shore-based analyses were placed in acid-washed plastic tubes and heat-sealed glass ampules.

IW samples were routinely analyzed for salinity as total dissolved solids with a Goldberg optical handheld refractometer (Reichart), for pH and alkalinity by Gran titration with a Brinkmann pH electrode and a Metrohm autotitrator, for dissolved chloride by titration, and for phosphate, nitrate, and ammonium by spectrophotometric methods with a Milton Roy Spectronic 301 spectrophotometer, following the analytical techniques described by Gieskes et al. (1991). International Association of Physical Sciences Organizations (IAPSO) standard seawater was used for calibrating most techniques. The reproducibility of these analyses, expressed as 1- σ standard deviations of the means of multiple determinations of IAPSO standard seawater or of a standard, are as follows: alkalinity, <1.5%; chloride, <0.2%; and phosphate, nitrate, and ammonium, 4%.

Potassium, calcium, magnesium, sodium, chloride, and sulfate were analyzed by ion chromatography using the Dionex DX100 ion chromatograph. The reproducibility of these analyses, expressed as 1- σ standard deviations of the means of multiple determinations of IAPSO standard seawater, are as follows: potassium, <2%; calcium, ~2%; magnesium, ~5%; and sulfate, ~1%. For sodium and chloride, the precision with the ion chromatograph is ~1% for Cl and <2% for Na but the accuracy for chloride by ion chromatography is lower than that obtained by titration.

ICP-AES Analyses

Fe, Mn, B, Li, and Sr concentrations in pore waters were determined by ICP-AES following the general procedure outlined by Murray et al. (2000). Chemical data for all interstitial waters are reported in molar units.

Inorganic Carbon

Inorganic carbon (IC) of sediment samples was determined using a Coulometrics 5011 carbon dioxide coulometer equipped with a System 140 carbonate carbon analyzer. A known mass, ranging from 18 to 20 mg of freeze-dried (dedicated carbonate samples) ground sediment was reacted in a 2-N HCl solution. The liberated CO₂ was titrated in a monoethanolamine solution with a colorimetric indicator; the change in light transmittance was monitored with a photodetection cell. The percentage of carbonate was calculated from the IC percentage content assuming that all carbonate is present as calcium carbonate:

$$\text{CaCO}_3 = \text{IC} \times 100/12.$$

The precision of these analyses, expressed as 1- σ standard deviations of the means of multiple determinations of a pure carbonate standard, is <1%.

Sediment residues were retained after acid digestion from carbonate analysis and washed several times with deionized water for subsequent CNS analysis. The purpose of this experimental procedure was to investigate whether these samples more accurately reflect concentrations of particulate (nonsulfate) sulfur.

Elemental Analysis

Total nitrogen, carbon, and sulfur in sediment samples were determined using a Carlo Erba Model NA1500 NCS analyzer. Mixtures of vanadium pentoxide and crushed freeze-dried samples (~5 mg) were combusted in an oxygen atmosphere at 1000°C, converting total (organic and inorganic) carbon to CO₂, sulfur to SO₂, and nitrogen to NO₂. The NO₂ was reduced to N₂ using copper. The gases were then separated by gas chromatography and measured with a thermal conductivity detector. The precision of these analyses, expressed as 1- σ standard deviations, is 2%–3%. Total organic carbon (TOC) was calculated by difference between total carbon (TC) from the NCS analyzer and IC from the coulometer:

$$\text{TOC} = \text{TC} - \text{IC}.$$

In addition, organic carbon was also measured directly from the acidified residues remaining from carbonate analysis.

Microbiological Analyses

In addition to the WRC samples taken for chemical analyses (above), WRC samples were also taken for microbiological analyses. These included 2-cm WRCs for postcruise lipid analyses, which were collected just below the intervals taken for IWs. These WRCs were immediately collected upon retrieval of the core on the catwalk before the end caps were sealed with acetone, placed in heat-sealed polyethylene bags, and frozen in the –86°C freezer. In addition, four WRCs were collected for microbial incubation experiments. A 15-cm whole-round sediment sample was collected at 5 mbsf from Hole 1179B, and 10-cm whole rounds were collected at 30, 100, and 200 mbsf from Holes 1179B and 1179C. These WRCs were also collected on the catwalk prior to acetone

application, capped, sealed with insulation tape, and immediately transferred to the anaerobic chamber for additional processing. In the case of the 30-mbsf sample, where there was a 3-hr delay between collection and processing, the capped and sealed sample was instead stored in the refrigerator until processing.

Processing of WRCs for Incubation Experiments

The anaerobic chamber had been prepared ahead of time by placing two large sheets of aluminum foil, one above the other, on the floor of the chamber. Both sheets were swabbed inside the chamber with 70% ethanol. Following this procedure, the gas inside the working and portal chambers was exchanged once with a mixture of gas containing 90% N₂, 5% H₂, and 5% CO₂. Autoclaved scalpels and spatulas had also been placed inside the chamber for processing of the core.

The capped WRC was placed inside the chamber. The outside liner was swabbed once with alcohol before extruding the core onto an unused and fresh portion of the aluminum foil. The core liner and caps were then removed from the working part of the chamber. In order to remove possible contaminants from the core, the ends were cut off and the sides were scraped with the autoclaved spatulas and scalpels. Between each scrape, the tools were swabbed with 70% ethanol and heated with an electric platinum wire inside the chamber. Once the entire core was prepared, the discarded sediment was wrapped inside the upper sheet of foil and removed from the working chamber. The lower sheet of foil was swabbed once more with 70% ethanol before the scraped core was transferred to this sheet for further processing.

Incubation experiments were designed to observe sulfate-reducing and methanogenic bacterial activity. From each WRC, ~50 replicate 20-mL serum vials were prepared, each containing 5-cm³ subsamples of the sediment. The serum vials and butyl-rubber stoppers had been autoclaved in advance. The subsamples were collected from the core with 5-mL presterile plastic syringes from which the luer end had been removed with a sterile scalpel blade. The 5- and 30-mbsf WRC subsamples could be pulled into the syringe by suction. In the 100- and 200-mbsf cores, where water porosity was noticeably lower, sediments could not be collected with suction. Instead, the plunger of the syringe was first withdrawn and the syringe barrel was immersed repeatedly into the core until it was filled. Either 6 or 16 mL of sterile filtered (0.2 μm) seawater (SW) was added to the different vials and subsequently crimp sealed with standard rubber and aluminum cap stoppers. The vials with 6 mL of SW added contained 10 mL of gas headspace that could be subsequently measured for changes in methane concentration with time from 1-mL subsamples of the gas headspace. Methane measurements were made onboard the ship using a Hewlett Packard gas chromatograph with a HayeSep Q column and flame ionization detector. Replicates of these vials were collected soon after setup in the anaerobic chamber and were immediately placed in the -86°C freezer to serve as the first "T-0" time point. The vials with 16 mL of sterile SW added had no gas headspace and were designed specifically for measuring sulfate reduction by the appearance of sulfide using an Orion ion-specific electrode. Because of slow response time of the electrode when used with sediment slurries, the sulfide measurements will be completed after the cruise from frozen samples.

For comparative purposes, the samples collected at 5, 30, and 100 mbsf were all incubated at 7°C. In situ temperatures, as determined

with an Adara temperature probe during coring, varied from ~2°C at the sediment/water interface to 8.2°C at 100 mbsf. Temperatures were not measured below 150 mbsf, where a temperature of ~11.5°C was measured. By extrapolation, a temperature of ~18°C was estimated for 200 mbsf. Therefore, incubation experiments from this depth were made at 20°C, as this was the lower limit of the only remaining and available incubator on board the ship.

Contamination Assays

To confirm the suitability of the core material for microbiological research, contamination assays were conducted to quantify the intrusion of drill water using the chemical tracer techniques that utilize perfluorocarbon tracers (PFTs) as described in ODP *Technical Note 28* (Smith et al., 2000). This was completed on Cores 191-1179B-5H and 191-1179C-21H. Each time, the second, fourth, and sixth sections of the core were sampled for subsequent PFT analysis. Samples for PFT analysis were taken from the cores using the sampling protocol described in ODP *Technical Note 28* (Smith et al., 2000). Unfortunately, an attempt to conduct PFT tests during XCB coring on Core 191-1179C-27H coincided with the contact of the chert layer, during which <1 m of sediment was collected, thus precluding PFT measurements.

IGNEOUS PETROLOGY

Core Curation and Shipboard Sampling

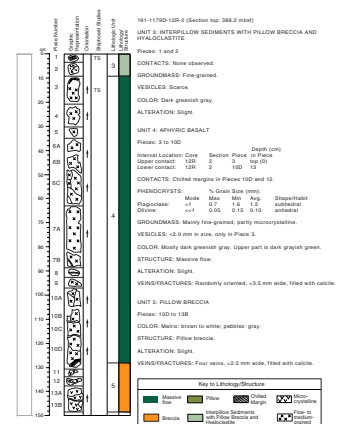
Each basement rock core was divided into 1.5-m sections. Each section was numbered, and each piece of rock in a section was numbered sequentially beginning with the number 1 at the top of each section. Pieces that could be fitted together were assigned the same number followed by a consecutive letter (e.g., 1A, 1B, 1C, etc.). Plastic spacers were placed between pieces having different numbers but not between pieces having the same number but different letters. The presence of a spacer represents an unknown, and possibly substantial, interval of no recovery. Any piece that was longer than the diameter of the core liner (i.e., the piece could not have rotated about a horizontal axis in the liner) was marked with a red wax arrow on the label pointing to the top of the section. Each piece was then split into archive and working halves using a rock saw with a diamond blade. Core descriptions, photographs, and nondestructive measurements were performed on the archive halves. Samples for shipboard analyses (physical properties, paleomagnetism, XRD, and thin-section studies) and shore-based analyses were taken from the working half of the core.

Visual Core Descriptions

Basement hard-rock cores were described on the VCD form (Fig. F4) specific to igneous rocks (see the “Core Descriptions” contents list). The VCD form for fine- and medium-grained igneous rocks includes the following information:

1. Leg, site, hole, core number and type, and section number;
2. A graphical representation of the core, including rock piece numbers and position of shipboard samples; and

F4. A sample igneous rock visual core description sheet, p. 41.



3. Position of lithostratigraphic unit boundaries, based on criteria such as the occurrence of glassy or quenched margins, marked trends of grain size variation, changes in petrographic type and phenocryst assemblages, and structural and textural variations. If the contact was recovered, its location was recorded by core, section, position (in centimeters), piece number, and unit number. When the contact was not recovered but a change of lithology was observed, the contact was placed at the base of the lowest piece in the lithostratigraphic unit.

The left column of the VCD is a graphical representation of the archive half. A horizontal line across the entire width of this column denotes a plastic spacer glued inside the liner. The number of each piece is also indicated. Oriented pieces are indicated by an upward-pointing arrow in the orientation of the appropriate piece. Samples for shipboard studies are indicated in the Shipboard Studies column, using the following notation:

XRD = X-ray diffraction analysis.
XRF = X-ray fluorescence analysis.
PMAG = magnetic measurements.
TS = thin section.

Core descriptions followed a checklist of macroscopic features to ensure consistent and complete descriptions. For each lithostratigraphic unit defined, the following checklist was used:

1. Unit: number (consecutive downhole), including piece numbers of top and bottom pieces in unit;
2. Rock name;
3. Contact type: intrusive, chilled, discordant, depositional, and so forth;
4. Phenocrysts: whether phenocrysts are homogeneous or heterogeneous through the unit. For each phenocryst phase, the following are listed: abundance (in percent), average size (in millimeters), shape (anhedral, subhedral, or euhedral), degree of alteration (in percent), and type of secondary phases.
5. Groundmass texture: glassy and/or cryptocrystalline (unable to identify), microcrystalline (unable to identify without microscope), fine grained (<1.0 mm), or medium grained (1.0–5.0 mm). Relative grain-size changes within a unit from piece to piece are noted.
6. Color (dry);
7. Vesicles: size, shape, percentage, distribution, and nature of any infillings;
8. Structure: massive flow, pillow, or brecciated;
9. Alteration: type, form, distribution, and degree, from fresh (<2% by volume alteration products), slight (2%–10%), moderate (>10%–40%), high (>40%–80%), very high (>80%–95%), or complete (>95%–100%); and
10. Veins/fractures: type, width, orientation, and nature of infillings.

Igneous rocks were named mainly on the basis of mineralogy and texture. Basalts (fine grained) and diabase (medium grained) were termed aphyric if they contained <1% phenocrysts. If porphyritic, the rock may

be sparsely phyric (phenocrysts content of 1%–2%), moderately phyric (>2%–10%), or highly phyric (>10%). Estimates of phenocryst proportions were based on those visible with a 10× hand lens. Basalts were further classified by phenocryst type: a moderately plagioclase-olivine phyric basalt contains >2%–10% total phenocrysts, most of which are plagioclase with lesser amounts of olivine.

Finally, any other miscellaneous comments were added, including continuity of the unit within the core and interrelationships among units. When the VCD form was complete, each record was checked by the database program for consistency and converted into a format that could be directly pasted onto the final VCD record for subsequent curatorial handling.

Thin-Section Descriptions

Petrographic descriptions, including estimates of the various mineral phases (both primary and secondary), were made on the igneous thin-section description form to complement the hand-specimen observations. Specifically, thin sections were used to describe (1) the texture and mineralogy of groundmass; (2) detail of phenocryst mineralogy including mineral type, morphology, size, and abundance; (3) the accessory minerals, such as chromium spinel, magnetite, zircon, and apatite, as well as the inclusions; and (4) the secondary mineral type, morphology, abundance, and the presence of vein vesicle and fracture filling. Identifications of very fine grained secondary phases, such as clays, zeolites, and infillings, were performed by XRD analysis. Modal data were collected using visual estimation by reference to standard charts. Crystal sizes were measured using a micrometer scale. A photomicrograph for each thin section was taken using a digital camera, and each picture was saved as a TIFF image file.

X-Ray Diffraction Analysis

A Philips PW1710 X-ray diffractometer was used for the XRD analysis of unknown, generally secondary, mineral phases. Instrument conditions were as follows: CuK_α radiation with monochromator, 40 kV, 35 mA, and goniometer step scan from 2° – $70^\circ 2\theta$ at steps of $0.02^\circ 2\theta/s$. Samples were ground with an agate mortar and pestle and mounted in aluminum sample holders. XRD data are compiled in a separate table in “Sedimentology,” p. 9, in the “Site 1179” chapter.

X-Ray Fluorescence Analysis

During Leg 191, problems with the ICP-AES on board prevented shipboard geochemical analysis of basaltic rocks. The XRF analysis of selected shipboard igneous rock samples was performed after the cruise at Hiroshima University. Results from these analysis are included in Table T10, p. 145, in the “Site 1179” chapter. We used a fully automated wavelength-dispersive Rigaku zsx-101e XRF system, equipped with a 3-kW generator and an Rh/W dual-anode X-ray tube, to determine the major and trace element abundances in the samples. Analytical conditions used are given in Table T1.

T1. Instrument conditions and analytical precision for XRF analyses, p. 46.

Sample Preparation

Following cutting by either a water-cooled diamond circular saw or a 1-in diameter diamond drill, the samples were polished using a diamond disk to remove saw marks or any unwanted material. The average sample taken weighed ~22 g. After polishing, the samples were cleaned in an ultrasonic bath in methanol and deionized water for 10 min each, followed by drying at 110°C. Larger pieces (~20 cm³) were reduced to <1 cm diameter by crushing between two disks of Delron plastic in a hydraulic press. The samples were then ground for ~1–5 min in a Spex 8510 shatterbox with a tungsten carbide barrel. We measured loss on ignition from weighed powders, which were heated for 2 hr at 1025°C. Fused glass discs were prepared for both major and trace element analysis using an alkali flux. The flux used was Johnson Matthey Spectroflux 100B, which is a mixture of lithium tetraborate (Li₂B₄O₇) and lithium metaborate (LiBO₂) with a mixing ratio of 2:8. The discs were prepared from 2.000 g of rock powder mixed with 4.000 g of dry flux. This mixture, with 0.6 g of LiNO₃ as an oxidizer and 100 µL of 5% LiI solution added to prevent adhesion to the Pt-Au crucible, was then melted in air at 1200°C for ~7 min with constant agitation to ensure thorough mixing and then cooled.

Calibration

Concentrations of all measured elements were computed from measured X-ray intensities using calibration curves derived from the measurement of 17 well-analyzed igneous rock reference standard samples provided by the Geological Survey of Japan (GSJ). The values recommended by Imai et al. (1995) are used for all elements. Data correction was made using the matrix effects compensation method, in which the matrix effects were corrected adopting the matrix compensation coefficients of major elements computed from the minute fluctuation method for theoretical X-ray intensity using the fundamental parameter method (Yamada et al., 1998). The analytical errors (relative standard deviation) based on the average of replicate analyses of the GSJ reference standard JB-1a are given in Table T1.

PALEOMAGNETISM

Introduction

The goals of paleomagnetic studies during Leg 191 were twofold: (1) to determine magnetic polarities of cores for correlation with the geomagnetic polarity time scale (GPTS) and (2) to measure paleomagnetic directions for tectonic studies. Paleomagnetic investigations during Leg 191 consisted of measurements of archive-half core sections and discrete samples taken from the working half of the core using the shipboard pass-through cryogenic magnetometer. Archive-half measurements were made for natural remanent magnetization (NRM) and remanent magnetization after alternating-field (AF) demagnetization. Whole-section measurements were made only on APC and XCB cores because of the internal rotation of core segments in RCB cores. Discrete samples were studied from the APC, XCB, and RCB cores. In the APC and XCB cores, discrete samples allowed a more detailed picture of the remanence to be developed. In the RCB cores, these samples were the sole source of

paleomagnetic information. To characterize magnetic carriers within the samples, isothermal remanent magnetization (IRM), anhysteretic remanent magnetization, and anisotropy of magnetic susceptibility (AMS) were measured in selected samples.

Paleomagnetic Instruments

A 2-G Enterprises pass-through cryogenic direct-current superconducting quantum interference device rock magnetometer (Model 760R) was used to make the majority of paleomagnetic measurements during Leg 191. This pass-through cryogenic magnetometer is equipped with an in-line AF demagnetizer (2-G Model 2G600) that allows for demagnetization of samples up to 80 mT. The magnetometer and AF demagnetizer are interfaced with a PC-compatible computer. The sensor coils of the cryogenic magnetometer measure a width of a little more than 30 cm, although ~85% of the remanence is sensed from a 20-cm width of a core section. A background resolution limit is imposed on measurement of rock remanence by the magnetization of the core liner itself, which is about 3×10^{-5} A/m.

Magnetic susceptibility of core sections was measured with two devices. Whole-core sections were measured on the whole-core MST. This apparatus includes a Bartington model MS2 meter with an 80-mm internal diameter MS2C sensor loop (88-mm coil diameter) operating at a frequency of 565 Hz and an AF of 80 A/m (0.1 mT). The specified sensitivity for the MS-2 susceptibility meter is 10^{-5} SI/10 cm³ volume or 10^{-8} SI/10 g mass. A second Bartington susceptibility meter is included on the AMST. This meter uses a 15-mm-diameter MS2F probe capable of making measurements of susceptibility at the core surface, giving a greater resolution than the loop sensor of the whole-core MST. The susceptibility sensitivity of the split-core meter is the same as the whole-core meter. Its specified horizontal resolution is 20 mm. Most of the probe sensitivity is within less than a diameter of the probe tip.

Additional instruments in the paleomagnetic laboratory include a DTECH model D-2000 AF demagnetizer capable of demagnetization up to 200 mT and a Schonstedt thermal demagnetizer (model TSD-1) capable of demagnetization up to 700°C. A Geofyzika Brno KLY-2 Kappa-bridge magnetic susceptibility meter, with an operating frequency of 920 Hz and a magnetic field intensity of 0.3 mT, allows measurements of the magnetic susceptibility and AMS of discrete samples. The specified magnetic susceptibility sensitivity of this instrument is 1×10^{-8} SI volume units, but the noisy environment of the core laboratory reduces the sensitivity to 1×10^{-6} SI. Also in the laboratory is an Analysis Services Company impulse magnetizer model IM-10, capable of applying magnetic fields from 0.02 to 1.35 T. This apparatus imparts an IRM on a sample, and the magnetization characteristics can be used to determine the type of magnetization carrier.

Tensor Orientation Tool

APC cores were oriented using the electronic tensor orientation tool. This instrument hooks to the sinker bar assembly above the core barrel, where it senses the magnetic field direction through a nonmagnetic drill collar. The tensor tool records the magnetic field direction every 30 s in internal memory. Valid orientation measurements were recognized by holding the drill string still for ~5 min while 6–10 consistent measurements were made before shooting the core. After the tensor tool

was recovered, orientation data were uploaded into a microcomputer and from there to the Janus database. Orientation corrections were made using the MTF angle (the angle between magnetic north and the double line on the core liner, which is at the base of the working half) in the following calculation:

$$D_t = D_{obs} + MTF + D_{ev}$$

where

- D_t = the corrected declination,
- D_{obs} = the measured direction in the core, and
- D_{ev} = the angle between true north and magnetic north at the site.

Paleomagnetic Measurements

Standard ODP paleomagnetic measurement conventions were used for Leg 191 paleomagnetic studies. The x-axis is positive upward (downward) from the split face of the archive (working) half of the core. The positive y-axis is left facing upcore along the split surface of the archive half, whereas the positive z-axis is downcore (Fig. F5).

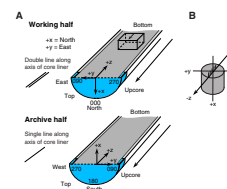
Each APC core archive half was routinely measured at 5-cm intervals using the shipboard pass-through cryogenic magnetometer. NRM was measured initially, followed by magnetization after progressive AF demagnetization at 10-mT steps from 10–50 mT. Demagnetization was accomplished using the in-line AF demagnetization coils built into the cryogenic magnetometer. Discrete samples were taken at intervals dictated by core recovery and scientific interest. These samples were usually either AF demagnetized at 5-mT intervals from 0 to 70 mT or thermally demagnetized at 50°C steps from 0° to 700°C.

Magnetic susceptibility measurements were made on APC cores with the MST and the AMST at 2-cm intervals. RCB samples were measured at 5-cm intervals. The quality of these results degraded in XCB and RCB sections, which can be undersized and/or disturbed. Nevertheless, the general downhole trends were useful for stratigraphic correlations. The MS2 meter measures relative susceptibilities that have not been corrected for the differences between core and coil diameters. Susceptibility values were stored in the Janus database as raw data in units of 10^{-5} SI. The true SI volume of susceptibilities should be multiplied by a correction factor to account for the volume of material that passed through the coils.

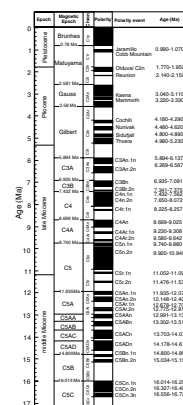
Geomagnetic Polarity Time Scales

Magnetic polarity results were correlated to the polarity reversal sequence, biostratigraphy and fossil stage boundaries, and absolute age using two primary GPTSs. For Cenozoic time, the Berggren et al. (1995b) geochronology was used (Fig. F6). This time scale incorporates the widely used calibration of age and polarity intervals derived by Cande and Kent (1995). For Mesozoic time, the GPTS of Gradstein et al. (1994, 1995) was employed.

F5. Coordinate systems of cores and discrete samples, p. 42.



F6. Miocene to Holocene geomagnetic polarity time scale, p. 43.



PHYSICAL PROPERTIES

Introduction

Shipboard measurements of physical properties are used for characterizing lithostratigraphic units, correlating cored material with down-hole logging data, and interpreting seismic reflection profiles.

After recovery, the cores are allowed to come to room temperature (22°–23°C) before thermal conductivity, bulk density, magnetic susceptibility (MS), compressional wave velocity, and natural gamma radiation (NGR) are measured in a series of nondestructive tests. Additional measurements of *P*-wave velocity, vane shear strength, bulk density, porosity, and water content are made on split cores or discrete samples.

Nondestructive Tests

Four sets of measurements, MS, gamma-ray attenuation (GRA) bulk density, *P*-wave velocity, and NGR are made in sequence on whole-core sections on the MST. MST data are sampled at discrete intervals, with the sampling intervals and count times chosen to optimize the resolution of the data in the time available to run each core section through the device. During Leg 191, MS, GRA bulk density, and NGR were measured on all APC and XCB cores. RCB cores were not passed through the MST because only fragments of chert or basalt were recovered; none of the intervening sediment survived the coring process.

Magnetic Susceptibility

The MST includes a Bartington susceptibility meter (model MS2C) that has an 8-cm loop and operates at 0.565 kHz with a field intensity of 80 A/m. Volume susceptibility, *k*, is a dimensionless measure of the degree to which material can be magnetized in an external magnetic field:

$$k = M/H,$$

where *M* is the magnetization induced in the material by an external field of strength *H*. Magnetic susceptibility is sensitive to variations of the type and content of magnetic grains in the sediment and is thus an indicator of compositional variations. During Leg 191, susceptibility was measured for 3 s on 2-cm intervals on all APC and XCB sections. Four-centimeter intervals at the top and bottom of each section were not sampled because of end effects.

Gamma-Ray Attenuation Bulk Density

GRA by Compton scattering is actually a measure of electron density. This method is useful for estimating the bulk densities of sediments and crystalline rocks because the ratio *Z/A* of atomic number/atomic mass of elements that make up the common rock-forming minerals is essentially constant (see Blum, 1997). Porosity is estimated from GRA bulk density by using an assumed grain density.

The GRA bulk densitometer measures the attenuation of a collimated beam of gamma-ray rays from a ¹³⁷Cs source as it passes through a sample of known thickness (Boyce, 1976). Having a well-known path length is critical to acquiring reliable GRA bulk densities, so the method

was restricted to APC and XCB cores, which usually fill the core liner. GRA bulk densitometer data were acquired during Leg 191 for 4 s at intervals of 2 cm, except for the top and bottom 2 cm of each section.

***P*-Wave Velocity**

Measured *P*-wave velocities are useful for interpreting seismic reflection profiles and correlating lithology with downhole sonic logs. The *P*-wave logger on the MST transmits a 500-kHz ultrasonic pulse through the core. Velocities are measured perpendicular to the long axis of the core, and a pair of displacement transducers is used to measure the separation between the compressional-wave transducers. During Leg 191, *P*-wave velocities were measured at 2-cm intervals on APC and XCB cores.

Natural Gamma Radiation

In nature, gamma-ray emissions result from the decay of the unstable elements ^{40}K , ^{232}Th , and ^{238}U . On the time scale of the measurements, these elements decay at constant rates, and the level of gamma-ray emissions depends on their concentration in the sediment. NGR emissions recorded in the laboratory can be correlated with the downhole measurements of natural gamma-ray emissions. The operating principles of the NGR system is described by Hoppie et al. (1994).

During Leg 191, NGR was measured for 60 s at intervals of 20 cm on all APC and XCB cores. The “area of influence” of the four NGR detectors is about ± 10 cm along the core axis from the point of measurement. As gamma-ray emission is a random event, count times have to be sufficiently long to average out short-period variations. Averaging is achieved on the MST by the long area of influence of the sensors and by applying a moving-average window to smooth count rate variations and to achieve a statistically valid measure of gamma-ray emissions.

The NGR was calibrated using a thorium source. Results are output in counts per second, which can be qualitatively compared to the American Petroleum Institute (API) units obtained from borehole logging.

Thermal Conductivity

Thermal conductivity is measured by transient heating of a material with a known heating power generated from a source of known geometry and then measuring the temperature change with time, using the TK04 system described by Blum (1997). Thermal conductivity profiles of sediments and rock sections are used along with temperature measurements to estimate heat flow. Heat flow varies with the age of oceanic crust and fluid circulation processes at depth (Blum, 1997). Whole-round core sections are allowed to adjust to room temperature for at least 2 hr in preparation for thermal conductivity measurements. In the case of soft sediments, thermal conductivity is measured on whole-core sections. The thermal conductivity of hard materials is measured on split-core pieces (working half). The needle probe method is used in full-space configuration for soft sediments (von Herzen and Maxwell, 1959) and in half-space mode (Vacquier, 1985) for lithified sediment and hard-rock samples. Measurements were made at an interval of one per core (whole-round or split core).

***P*-Wave Velocity (W-Logger)**

In comparatively soft sediments, *P*-wave velocities are measured in three directions using the PWS1, PWS2, and PWS3 (Hamilton Frame) systems. The PWS3 is also used to measure velocities in hard-sediment split cores and in discrete samples (cut cores and cubes) of harder sediments or crystalline rocks.

The PWS1 and PWS2 systems measure *P*-wave velocities using two pairs of digital sound velocimeters that are inserted in soft sediments. One pair (PWS1) is aligned with the core axis (the *z*-direction, normal to bedding), and the other (PWS2) is aligned perpendicular to the core axis (in the *y*-direction, parallel to bedding). The transducer pairs have fixed separations of 7 cm (vertical) and 3.5 cm (horizontal), respectively. The received 500-kHz ultrasonic signal is digitized by an oscilloscope; the first arrival is picked automatically or manually using a threshold criterion, and the velocity is calculated from the transducer separation and the propagation time.

The PWS3 system is a modified and updated version of the classic Hamilton Frame velocimeter, in which one transducer is fixed and the other is mounted on a screw. The PWS3 is mounted vertically to measure velocities in the *x*-direction (i.e., perpendicular to both the core axis and PWS2). The PWS3 can be used to measure *P*-wave velocities in either discrete samples or split cores by placing the sample or the core liner on the lower transducer and bringing the upper transducer into direct contact with the upper surface. To improve the coupling (i.e., the impedance match) between the transducer and the sample, water is commonly applied to the top and bottom of the sample and transducer heads. Traveltimes are picked manually or automatically by the threshold method as described above, and the transducer separation is recorded by a digital caliper. Measurements on split cores are corrected for the additional path length and traveltime of the core liner. During Leg 191, *P*-wave velocities were measured on each APC and XCB split-core section and in a number of discrete samples of basalt recovered from basement.

Undrained Shear Strength

The peak undrained and residual shear strength of soft sediment was measured at an interval of one per split-core section using a Wykeham-Farrance motorized vane shear apparatus following procedures described by Boyce (1977). The vane rotation rate was set to 90°/min, and the vane used for all measurements had a 1:1 blade ratio with a dimension of 1.28 cm. The vane shear instrument measures the torque and strain at the vane shaft using a torque transducer and potentiometer. The reported shear strength is the peak strength determined from the torque vs. strain analysis.

Interpretations of vane shear measurements assume that a cylinder of sediment is uniformly sheared around the axis of the vane in an undrained condition, with cohesion as the principal contributor to shear strength. Departures from this assumption include progressive cracking within and outside of the failing specimen, uplift of the failing core cylinder, drainage of local pore pressures, and stick-slip behavior.

Index Properties

Samples of ~10 cm³ were taken from each APC and XCB sediment section to measure the index properties. Bulk density, grain density, water content, porosity, and dry density were usually calculated from wet and dry sample weights and dry volumes. In a few cores, density and porosity were estimated from the wet and dry sample weights and the wet sample volume. Sample mass is determined to a precision of ±0.001 g using two Scitech electronic balances. The balances are equipped with a computer averaging system that compensates for the motion of the ship. The sample mass on one balance is counterbalanced by a known mass on the adjacent balance. Sample volumes are determined using a five-cell Quantachrome Penta-Pycnometer helium-displacement pycnometer with a nominal precision of ±0.01 cm³. Sample volumes are measured at least three times and then averaged. A standard reference sphere is run sequentially in each of the five operating cells to maintain calibration. The cell volume is recalibrated if the measured volume of the standard is not within 0.02 cm³ of the known volume of the standard. The beakers that are used for soft sediment samples were calibrated before the cruise. Dry weight and volume measurements were performed after the samples were oven dried at 105° ± 5°C for 24 hr and allowed to cool in a desiccator. A potential problem with this drying temperature is that chemically bound water in some clay minerals can be lost along with interstitial water.

Water Content

Water content as a fraction of total mass or as a ratio of water mass to solid mass is determined by standard methods of the American Society for Testing and Materials (ASTM) designation (D) 2216 (ASTM, 1989). The total (water saturated) mass (M_t) and dry mass (M_d) are measured using the electronic balance as described above, and the difference is taken as the uncorrected water mass. Measured wet and dry masses are corrected for salt assuming a pore-water salinity (r) of 0.35% (Boyce, 1976). The wet and dry water contents (W_d and W_w [in percent]) are given, respectively, by

$$W_d = [(M_t - M_d)/(M_d - rM_t)] \times 100 \text{ and}$$

$$W_w = \{(M_t - M_d)/[(1 - r) \times M_t]\} \times 100.$$

Bulk Density

Bulk density (ρ_b), in grams per cubic centimeter, is the density of the saturated sample,

$$\rho_b = M_t/V_t$$

where

V_t = total sample volume, and

M_t = water-saturated mass.

Grain Density

Grain density (ρ_g), in grams per cubic centimeter, is determined from the dry mass and dry volume measurements. Both mass and volume must be corrected for the salt content of the pore fluid:

$$\rho_g = (M_d - M_s) / [V_d - (M_s / \rho_s)],$$

where

M_d = the dry mass (in grams),
 ρ_s = the density of salt (2.257 g/cm³),
 $M_s = rM_w$; the mass of salt in the pore fluid, and
 M_w = the salt-corrected mass of the seawater:

$$M_w = (M_t - M_d) / (1 - r).$$

Porosity

Porosity (Φ) is the ratio of pore-water volume to total volume and can be calculated from the fluid density, grain density, and bulk density of the material:

$$\Phi = [(\rho_g - \rho_b) / (\rho_g - \rho_w)] \times 100,$$

where

ρ_g = grain density,
 ρ_b = bulk density, and
 ρ_w = density the pore fluid, which is assumed to be seawater.

Dry Density

The dry density (ρ_d) is the ratio of the dry mass (M_d) to the total volume (V_t). The dry density is calculated from the corrected water content (W_d) and porosity (Φ):

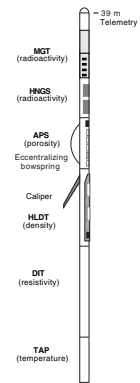
$$\rho_d = (\Phi / W_d) \times \rho_w$$

DOWNHOLE MEASUREMENTS

Introduction

Downhole logs are continuous in situ records of physical and structural properties of the formation penetrated by a borehole. The logs are made using a variety of probes combined into tool strings (Fig. F7). These strings can be lowered down the hole on a heave-compensated electrical wireline and then pulled up at constant speed to provide continuous measurements, as a function of depth, of several properties simultaneously. Logs can be used to interpret the structure, stratigraphy, lithology, and mineral composition of the penetrated formation. Where core recovery is incomplete or disturbed, log data may provide the only way to characterize the borehole section. Where core recovery is good,

F7. The triple-combination tool string, p. 44.



log and core data complement one another and may be interpreted jointly.

Logging Tools

Owing to unstable conditions in the only hole logged during Leg 191, only one tool string was run: the triple combination (triple combo), which measures resistivity, density, and porosity (Fig. F7). This tool consists of the accelerator porosity sonde (APS), the hostile environment natural gamma-ray sonde (HNGS), the high-temperature lithodensity tool (HLDT), and the phasor dual induction-spherically focused resistivity tool (DIT). The Lamont multisensor gamma-ray tool (MGT) (Fig. F8) and universal data telemetry module (UDTM) were included at the top of the tool string. A downhole cable switch in the UDTM allowed simultaneous deployment and cable line switching between the MGT and Schlumberger tool strings. The Lamont-Doherty Earth Observatory (LDEO) temperature/acceleration/pressure (TAP) tool was attached to the bottom of the tool string.

Each tool string includes a telemetry cartridge for communicating through the wireline with the logging laboratory on the drillship and a natural gamma-ray sonde that is used to identify lithologic markers, providing a common reference for correlation and depth shifting between multiple logging runs.

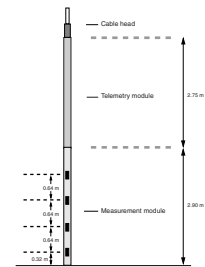
The principal data outputs of the standard logging tools, their physical significance, and units of measure are listed in Table T2. The logging tools are briefly described below, and their operating principles, applications, and approximate vertical resolution are summarized in Table T3. More detailed information on individual tools and their geological applications may be found in Ellis (1987), Goldberg (1997), Rider (1996), Schlumberger (1989, 1994), Serra (1984, 1986, 1989), and at the Borehole Research Group Web site (see the “[Related Leg Data](#)” contents list).

Natural Radioactivity

Three spectral gamma-ray tools were used to measure and classify natural radioactivity in the formation: the HNGS, natural gamma spectrometry tool (NGT), and MGT. The NGT uses a sodium iodide scintillation detector and five-window spectroscopy to determine concentrations of K (in weight percent), Th (in parts per million), and U (in parts per million), the three elements whose isotopes dominate the natural gamma radiation spectrum. The HNGS is similar to the NGT, but it uses two bismuth germanate scintillation detectors for significantly improved tool precision. Spectral analysis of the HNGS data filters out gamma-ray energies below 500 keV, eliminating sensitivity to bentonite or KCl in the drilling mud and improving measurement accuracy. Because NGT response is sensitive to borehole diameter and the weight and concentration of bentonite or KCl present in the drilling mud, corrections are routinely made for these effects during processing at LDEO.

The newly developed LDEO MGT was tested as a part of the triple-combo tool string (Fig. F7). The major advantage of the new tool is improved vertical resolution, comparable with the resolution of MST core measurements. This is achieved by real-time stacking of NGR spectral data from four independent small-sized scintillation detectors positioned at 0.64-m spacing in the measurement module (Fig. F8). The tool provides 256-channel spectral analysis of each detector data in the

F8. Schematic diagram of the multisensor gamma-ray tool, p. 45.



T2. Logging tools application and acronyms, p. 47.

T3. Principal channels of logging tools, p. 48.

0.2- to 3.0-MeV energy range. The full spectra are later combined into five- or three-window spectral data for compatibility with the older tools. The total gamma (in API units) and concentrations of K (in weight percent), Th (in parts per million), and U (in parts per million) are calculated in real time either from spectral data of individual detectors or from stacked data. The tool also includes an accelerometer for precise depth correction in the process of data stacking.

Density

Formation density was determined from the density of electrons in the formation, which was measured with the HLDT. The sonde contains a radioactive cesium (^{137}Cs) gamma-ray source (622 keV) and far and near gamma-ray detectors mounted on a shielded skid that is pressed against the borehole wall by a hydraulically activated eccentralizing arm. Gamma rays emitted by the source experience Compton scattering, which involves the transfer of energy from gamma rays to the electrons in the formation by elastic collision. The number of scattered gamma rays that reach the detectors is directly related to the number of electrons in the formation, which is in turn related to bulk density. Porosity may also be derived from this bulk density if the matrix density is known.

The HLDT also measures the photoelectric effect factor (PEF) caused by absorption of low-energy gamma rays. Photoelectric absorption occurs when gamma rays reach <150 keV after being repeatedly scattered by electrons in the formation. Photoelectric absorption is strongly dependent on the atomic number of the constituents of the formation; it varies according to the chemical composition and is essentially independent of porosity. For example, the PEF of pure calcite = 5.08, illite = 3.03, quartz = 1.81, and kaolinite = 1.49 barn/e⁻. PEF values can be used in combination with NGT curves to identify different types of clay minerals. The PEF values, therefore, can give an indication of the chemical composition of the rock.

Coupling between the tool and borehole wall is essential for good HLDT logs. Poor contact results in underestimation of density values.

Porosity

Formation porosity was measured with the APS. The sonde incorporates a minitron neutron generator, which produces fast (14.4 MeV) neutrons, and five neutron detectors (four epithermal and one thermal) positioned at different spacings. The tool is pressed against the borehole wall by an eccentralizing bowspring. Emitted neutrons are slowed by collisions. The amount of energy lost per collision depends on the relative mass of the nucleus with which the neutron collides. The greatest energy loss occurs when the neutron strikes a nucleus nearly equal to its own mass, such as in the case of hydrogen, which is mainly present in the pore water. The neutron detectors record both the numbers of neutrons arriving at various distances from the source and neutron arrival times that act as a measure of formation porosity. However, as hydrogen bound in minerals such as clays or in hydrocarbons also contributes to the measurement, the raw porosity value is often an overestimate.

Electrical Resistivity

The DIT measures the formation electrical resistivity and provides three different measurements of electrical resistivity based on multiple depths of investigation: deep induction, medium induction, and shallow spherically focused resistivity. Deep- and medium-penetration measurements are made inductively using transmitter coils that are energized with high-frequency alternating currents, creating time-varying magnetic fields that induce secondary Foucault currents in the formation. The strength of these induced ground currents is inversely proportional to the resistivity of the formation through which they circulate, as are the secondary inductive fields that they create. The amplitude and phase of the secondary magnetic fields, measured with receiving coils, are used as a proxy for the formation resistivity. Shallow penetration measurements with a high vertical resolution are made with a spherically focused laterolog. This measures the current necessary to maintain a constant voltage drop across a small fixed interval. Because the solid constituents of rocks are essentially infinitely resistive relative to the pore fluids, resistivity is controlled mainly by the nature of the pore fluids, porosity, and permeability.

In most rocks, electrical conduction occurs primarily by ion transport through pore fluids and is strongly dependent on porosity. Electrical resistivity data can therefore be used to estimate formation porosity using Archie's Law (Archie, 1942) if the formation does not contain clay. Archie's Law is expressed as

$$FF = \alpha \phi^{-m},$$

where

FF = formation factor (i.e., the ratio of the formation resistivity to that of the pore fluids),

ϕ = porosity,

m = cementation factor that depends on the tortuosity and connectivity of pore spaces, and

α = a constant that varies with rock type.

Temperature, Acceleration, and Pressure

Downhole temperature, acceleration, and pressure were measured with the LDEO high-resolution TAP tool. When attached to the bottom of the triple-combo string, the TAP operates in an autonomous mode, with data stored in built-in memory. A two-component thermistor (for different temperature ranges) is mounted near the bottom of the tool in the slotted protective cover. The time constant of the thermistor assembly in the water is ~0.4 s. The tool also includes a pressure transducer (0–10,000 psi), which is used to activate the tool at a specified depth to perform pressure measurements. The TAP tool also incorporates a high-sensitivity vertical accelerometer, providing data for analyzing the effects of heave on a deployed tool string, and an internal temperature sensor for monitoring the temperature inside the electronics cartridge. Temperature and pressure data are recorded once per second, and accelerometer data can be recorded at 4- or 8-Hz sampling rate.

The borehole temperature record provides information on the thermal regime of the surrounding formation. The vertical heat flow can be estimated from the vertical temperature gradient combined with mea-

surements of the thermal conductivity from core samples and conductive heat transfer regimes.

The temperature record must be interpreted with caution, as the amount of time elapsed between the end of drilling and the logging operation is generally not sufficient to allow the borehole to recover thermally from the influence of drilling fluid circulation. The data recorded under such circumstances may differ significantly from the thermal equilibrium of that environment. Nevertheless, from the spatial temperature gradient, it is possible to identify abrupt temperature changes that may represent localized fluid flow into the borehole indicative of fluid pathways and fracturing and/or breaks in the temperature gradient that may correspond to contrasts in permeability at lithologic contacts.

Log Data Quality

The quality of log data may be seriously degraded by excessively wide sections of the borehole or by rapid changes in the hole diameter. Resistivity and velocity measurements are the least sensitive to borehole effects, whereas the nuclear measurements (density, neutron porosity, and both natural and induced spectral gamma rays) are most sensitive because of the large attenuation by borehole fluid. Corrections can be applied to the original data to reduce the effects of these conditions, and generally, any departure from the conditions under which the tool was calibrated.

Logs from different tool strings may have depth mismatches, caused by either cable stretch or ship heave during recording. Small errors in depth matching can distort the logging results in zones of rapidly changing lithology. To minimize the effects of ship heave, a hydraulic wireline heave compensator adjusts for rig motion during logging operations. Distinctive features recorded by the NGT, run on every log tool string, provide correlation and relative depth offsets among the logging runs and can be calibrated to distinctive lithologic contacts observed in the core recovery or drilling penetration (e.g., basement contacts).

Data Recording and Processing

Data for each logging run were recorded, stored digitally, and monitored in real time using the Schlumberger minimum configuration maxis. On completion of logging at each hole, data were transferred to the downhole measurements laboratory for preliminary interpretation. Basic processing is then carried out in order to provide scientists with a comprehensive, quality controlled downhole log data set that can be used for comparison and integration with other data collected during each ODP leg. This processing is usually carried out onshore at LDEO after the data are transmitted by satellite from the ship. It includes: depth adjustments to remove depth offsets between data from different logging runs, corrections specific to certain tools and logs, documentation for the logs with an assessment of log quality, and conversion of the data to a widely accessible format (ASCII for conventional logs). Schlumberger GeoQuest's GeoFrame software package is used for most of the processing.

Processed acoustic, caliper, density, gamma-ray, magnetic, neutron porosity, resistivity, and temperature data in ASCII format will be available directly from the LDEO-BRG Web site (see the ["Related Leg Data"](#)

contents list). A summary of logging highlights is also posted on the LDEO-BRG web site at the end of each leg.

Drill String Acceleration Measurements Tool

The drill string acceleration (DSA) measurement tool was an experimental device deployed during Leg 191. The DSA tool attaches to the core barrel and records drill string acceleration in two frequency bands during the process of coring. The acquired data may be used for drill string vibration analysis, heave evaluation, and as a reference signal for seismic-while-drilling measurements. The DSA tool operates as a memory tool, recording the tool's acceleration, ambient pressure, and internal temperature. The tool uses two accelerometers: an axial (vertical) high-sensitivity accelerometer (HSA), and a three-axis low-sensitivity accelerometer. The DSA can operate either in heave mode (only the HSA signal is recorded) or in drill mode (both accelerometer signals are recorded).

The tool does not require connection to the logging cable and the data can be offloaded to a computer after the tool is retrieved from the hole.

REFERENCES

- Archie, G.E., 1942. The electrical resistivity log as an aid in determining some reservoir characteristics. *J. Pet. Technol.*, 5:1–8.
- ASTM, 1989. *Annual Book of ASTM Standards for Soil and Rock: Building Stones* (Vol. 4.08): *Geotextiles*: Philadelphia (Am. Soc. Testing and Mater.).
- Baccelle, L., and Bosellini, A., 1965. Diagrammi per la stima visiva della composizione percentuale nelle rocce sedimentarie. *Ann. Univ. Ferrara, N. Ser., Sez. IX, Sci. Geol. Paleontol.*, 1:59–62.
- Balsam, W.L., and Damuth, J.E., 2000. Further investigations of shipboard vs. shore-based spectral data: implications for interpreting Leg 164 sediment composition. In Paull, C.K., Matsumoto, R., Wallace, P., and Dillon, W.P. (Eds.), *Proc. ODP, Init. Repts.*, 164: College Station, TX (Ocean Drilling Program), 313–324.
- Balsam, W.L., Damuth, J.E., and Schneider, R.R., 1997. Comparison of shipboard vs. shore-based spectral data from Amazon Fan cores: implications for interpreting sediment composition. In Flood, R.D., Piper, D.J.W., Klaus, A., and Peterson, L.C. (Eds.), *Proc. ODP, Sci. Results*, 155: College Station, TX (Ocean Drilling Program), 193–215.
- Balsam, W.L., Deaton, B.C., and Damuth, J.E., 1998. The effects of water content on diffuse reflectance measurements of deep-sea core samples: an example from ODP Leg 164 sediments. *Mar. Geol.*, 149:177–189.
- Berggren, W.A., Kent, D.V., Aubry, M.-P., and Hardenbol, J., 1995a. Geochronology, time scales and global stratigraphic correlation: unified temporal framework for an historical geology. In Berggren, W.A., Kent, D.V., Aubry, M.-P., and Hardenbol, J. (Eds.), *Geochronology, Time Scales and Global Stratigraphic Correlation*. Spec. Publ.—Soc. Econ. Paleontol. Mineral., 54:v–vi.
- Berggren, W.A., Kent, D.V., Swisher, C.C., III, and Aubry, M.-P., 1995b. A revised Cenozoic geochronology and chronostratigraphy. In Berggren, W.A., Kent, D.V., Aubry, M.-P., and Hardenbol, J. (Eds.), *Geochronology, Time Scales and Global Stratigraphic Correlation*. Spec. Publ.—Soc. Econ. Paleontol. Mineral. (Soc. Sediment. Geol.), 54:129–212.
- Blum, P., 1997. Physical properties handbook: a guide to the shipboard measurement of physical properties of deep-sea cores. *ODP Tech. Note*, 26 [Online]. Available from World Wide Web: <<http://www-odp.tamu.edu/publications/tnotes/tn26/INDEX.HTM>>. [Cited 2000-07-16] [N1]
- Boyce, R.E., 1976. Definitions and laboratory techniques of compressional sound velocity parameters and wet-water content, wet-bulk density, and porosity parameters by gravimetric and gamma-ray attenuation techniques. In Schlanger, S.O., Jackson, E.D., et al., *Init. Repts. DSDP*, 33: Washington (U.S. Govt. Printing Office), 931–958.
- , 1977. Deep Sea Drilling Project procedures for shear strength measurement of clayey sediment using modified Wykeham Farrance laboratory vane apparatus. In Barker, P.F., Dalziel, I.W.D., et al., *Init. Repts. DSDP*, 36: Washington (U.S. Govt. Printing Office), 1059–1068.
- Cande, S.C., and Kent, D.V., 1995. Revised calibration of the geomagnetic polarity timescale for the Late Cretaceous and Cenozoic. *J. Geophys. Res.*, 100:6093–6095.
- de Verteuil, L., 1996. Data report: Upper Cenozoic dinoflagellate cysts from the continental slope and rise off New Jersey. In Mountain, G.S., Miller, K.G., Blum, P., Poag, C.W., and Twichell, D.C. (Eds.), *Proc. ODP, Sci. Results*, 150: College Station, TX (Ocean Drilling Program), 439–454.
- Doeglas, D.J., 1968. Grain-size indices, classification and environment. *Sedimentology*, 10:83–100.
- Ellis, D.V., 1987. *Well Logging for Earth Scientists*: New York (Elsevier).
- Flügel, E., 1982. *Microfacies Analysis of Limestones*: New York (Springer-Verlag).
- Folk, R.L., 1980. *Petrology of Sedimentary Rocks* (2nd ed.): Austin, TX (Hemphill Publ.).

- Gieskes, J.M., Gamo, T., and Brumsack, H., 1991. Chemical methods for interstitial water analysis aboard *JOIDES Resolution*. *ODP Tech. Note*, 15 [Online]. Available from World Wide Web: <http://www-odp.tamu.edu/publications/tnotes/tn15/f_chem1.htm>. [Cited 2000-07-16] [N1]
- Goldberg, D., 1997. The role of downhole measurements in marine geology and geophysics. *Rev. Geophys.*, 35:315–342.
- Gradstein, F.M., Agterberg, F.P., Ogg, J.G., Hardenbol, J., van Veen, P., Thierry, J., and Huang, Z., 1994. A Mesozoic time scale. *J. Geophys. Res.*, 99:24051–24074.
- , 1995. A Triassic, Jurassic and Cretaceous time scale. In Berggren, W.A., Kent, D.V., and Aubry, M.P., and Hardenbol, J. (Eds.), *Geochronology, Time Scales and Global Stratigraphic Correlation*. Spec. Publ.—Soc. Econ. Paleontol. Mineral., 54:95–126.
- Harland, R., 1992. Dinoflagellate cysts of the Quaternary System. In Powell, A.J. (Ed.), *A Stratigraphic Index of Dinoflagellate Cysts*: London (Chapman Hall), 253–273.
- Hoppie, B.W., Blum, P., and the Shipboard Scientific Party, 1994. Natural gamma-ray measurements on ODP cores: introduction to procedures with examples from Leg 150. In Mountain, G.S., Miller, K.G., Blum, P., et al., *Proc. ODP, Init. Repts.*, 150: College Station, TX (Ocean Drilling Program), 51–59.
- Imai, N., Terashima, S., Itoh, S., and Ando, A., 1995. 1994 compilation values for GSI reference samples, igneous rock series. *Geochem. J.*, 29:91–95.
- Ingram, R.L., 1954. Terminology for the thickness of stratification and parting units in sedimentary rocks. *Geol. Soc. Am. Bull.*, 65:937–938.
- Isaacs, C.M., 1982. Influence of rock compositions on kinetics of silica phase changes in the Monterey Formation, Santa Barbara area, California. *Geology*, 10:304–308.
- Isaacs, C.M., Pisciotto, K.A., and Garrison, R.E., 1983. Facies and diagenesis of the Miocene Monterey Formation, California: a summary. In Iijima, A., Hein, J.R., and Siever, R. (Eds.), *Siliceous Deposits in the Pacific Region*: Amsterdam (Elsevier), *Devl. in Sedimentol. Ser.*, 36:247–282.
- Loeblich, A.R., Jr., and Tappan, H., 1988. *Foraminiferal Genera and Their Classification*: New York (Van Nostrand Reinhold).
- Manheim, F.T., and Sayles, F.L., 1974. Composition and origin of interstitial waters of marine sediments, based on deep sea drill cores. In Goldberg, E.D. (Ed.), *The Sea* (Vol. 5): *Marine Chemistry: The Sedimentary Cycle*: New York (Wiley), 527–568.
- Martini, E., 1971. Standard Tertiary and Quaternary calcareous nannoplankton zonation. In Farinacci, A. (Ed.), *Proc. 2nd Int. Conf. Planktonic Microfossils Roma*: Rome (Ed. Tecnosci.), 2:739–785.
- Matsuoka, K., 1983. Late Cenozoic dinoflagellates and acritarchs in the Niigata District, Central Japan. *Palaeontographica B*, 187:89–154.
- Mazzullo, J., and Graham, A.G. (Eds.), 1988. *Handbook for Shipboard Sedimentologists*. ODP Tech. Note, 8.
- Mazzullo, J.M., Meyer, A., and Kidd, R.B., 1988. New sediment classification scheme for the Ocean Drilling Program. In Mazzullo, J., and Graham, A.G. (Eds.), *Handbook for Shipboard Sedimentologists*. ODP Tech. Note, 8:45–67.
- McCarthy, F.M.G., Gostlin, K.E., Mudie, P.J., and Scott, D.B., 2000. Synchronous palynological changes in early Pleistocene sediments off New Jersey and Iberia and a possible paleoceanographic explanation. *Palynology*, 24:63–77.
- McCarthy, F.M.G., and Mudie, P.J., 1996. Palynology and dinoflagellate biostratigraphy of upper Cenozoic sediments from Sites 898 and 900, Iberia Abyssal Plain. In Whitmarsh, R.B., Sawyer, D.S., Klaus, A., and Masson, D.G. (Eds.), *Proc. ODP, Sci. Results*, 149: College Station, TX (Ocean Drilling Program), 241–265.
- McKee, E.D., and Weir, G.W., 1953. Terminology for stratification and cross-stratification in sedimentary rocks. *Geol. Soc. Am. Bull.*, 64:381–390.
- Mudie, P.J., 1987. Palynology and dinoflagellate biostratigraphy of Deep Sea Drilling Project Leg 94, Sites 607 and 611, North Atlantic Ocean. In Ruddiman, W.F., Kidd, R.B., Thomas, E., et al., *Init. Repts. DSDP*, 94 (Pt. 2): Washington (U.S. Govt. Printing Office), 785–812.

- Munsell Color Company, Inc., 1975. *Munsell Soil Color Charts*: Baltimore, MD (Munsell).
- Murray, R.W., Miller, D.J., and Kryc, K.A., 2000. Analysis of major and trace elements in rocks, sediments, and interstitial waters by inductively coupled plasma-atomic emission spectrometry (ICP-AES). *ODP Tech. Note, 29* [Online]. Available from World Wide Web: <<http://www-odp.tamu.edu/publications/tnotes/tn29/INDEX.HTM>>. [Cited 2000-07-16]
- Okada, H., and Bukry, D., 1980. Supplementary modification and introduction of code numbers to the low-latitude coccolith biostratigraphic zonation (Bukry, 1973; 1975). *Mar. Micropaleontol.*, 5:321–325.
- Perch-Nielsen, K., 1983. Recognition of Cretaceous stage boundaries by means of calcareous nannofossils. In Birkelund, T., et al. (Eds.), *Symposium on Cretaceous Stage Boundaries, Copenhagen*, 152–156. (Abstract)
- Powell, A.J., 1992. Dinoflagellate cysts of the Tertiary System. In Powell, A.J. (Ed.), *A Stratigraphic Index of Dinoflagellate Cysts*: London (Chapman and Hall), 155–251.
- Rider, M., 1996. *The Geological Interpretation of Well Logs* (2nd ed.): Caithness (Whittles Publishing).
- Rock-Color Chart Committee, 1991. *Rock Color Charts*. Geol. Soc. Am.
- Schlumberger, 1989. *Log Interpretation Principles/Applications*: Houston (Schlumberger Educ. Services), SMP-7017.
- , 1994. *IPL Integrated Porosity Lithology*: Houston (Schlumberger Wireline and Testing), SMP-9270.
- Serra, O., 1984. *Fundamentals of Well-Log Interpretation* (Vol. 1): *The Acquisition of Logging Data*: Dev. Pet. Sci., 15A.
- , 1986. *Fundamentals of Well-Log Interpretation* (Vol. 2): *The Interpretation of Logging Data*. Dev. Pet. Sci., 15B.
- , 1989. *Formation MicroScanner Image Interpretation*: Houston (Schlumberger Educ. Services), SMP-7028.
- Shipboard Scientific Party, 1998a. Explanatory notes. In Norris, R.D., Kroon, D., Klaus, A., et al., *Proc. ODP, Init. Repts.*, 171B: College Station, TX (Ocean Drilling Program), 11–44.
- , 1998b. Explanatory notes. In Wefer, G., Berger, W.H., and Richter, C., et al., *Proc. ODP, Init. Repts.*, 175: College Station, TX (Ocean Drilling Program), 27–46.
- , 1998c. Explanatory notes. In Whitmarsh, R.B., Beslier, M.-O., Wallace, P.J., et al., *Proc. ODP, Init. Repts.*, 173: College Station, TX (Ocean Drilling Program), 25–47.
- , 2000. Explanatory notes. In Plank, T., Ludden, J.N., Escutia C., et al., *Proc. ODP, Init. Repts.*, 185, 1–76 [CD-ROM]. Available from: Ocean Drilling Program, Texas A&M University, College Station TX 77845-9547, USA.
- Smith, D.C., Spivack, A.J., Fisk, M.R., Haveman, S.A., Staudigel, H., and the Leg 185 Shipboard Scientific Party, 2000. Methods for quantifying potential microbial contamination during deep ocean coring. *ODP Tech. Note, 28* [Online]. Available from World Wide Web: <<http://www-odp.tamu.edu/publications/tnotes/tn28/INDEX.HTM>>. [Cited 2000-07-16]
- Stockmarr, J., 1971. Tablets with spores used in absolute pollen analysis. *Pollen et Spores*, 13:615–621.
- Vacquier, V., 1985. The measurement of thermal conductivity of solids with a transient linear heat source on the plane surface of a poorly conducting body. *Earth Planet. Sci. Lett.*, 74:275–279.
- van Andel, T., 1983. Sediment nomenclature and classification. In Heath, G.R. (Ed.), *Sedimentology, Physical Properties, and Geochemistry in the Initial Reports of the Deep Sea Drilling Project Volumes 1-44: An Overview*: Boulder, Colorado (U.S. Dept. of Commerce, National Oceanic and Atmospheric Administration, Environmental Data and Information Service), World Data Center A for Marine Geology and Geophysics, Rep. MGG-1:3–25.

- Von Herzen, R.P., and Maxwell, A.E., 1959. The measurement of thermal conductivity of deep-sea sediments by a needle-probe method. *J. Geophys. Res.*, 64:1557–1563.
- Wessel, P., and Smith, W.H.F., 1995. New version of the Generic Mapping Tools released. *Eos*, 76:329.
- Williams, G.L., Stover, L.E., and Kidson, E.J., 1993. Morphology and Stratigraphic Ranges of Selected Mesozoic-Cenozoic Dinoflagellate Taxa in the Northern Hemisphere. *Pap.—Geol. Surv. Can.*, 92-10.
- Yamada, Y., Kohno, H., Shiraki, K., Nagao, T., Kakubuchi, S., Oba, T., Kawate, S., and Murata, M., 1998. Analysis of major, trace and rare earth elements in geological samples using low dilution glass bead. *Adv. X-Ray Anal.*, 29:47–70. (in Japanese with English abstract)

Figure F1. Illustration of hole, core, section, and sample numbering.

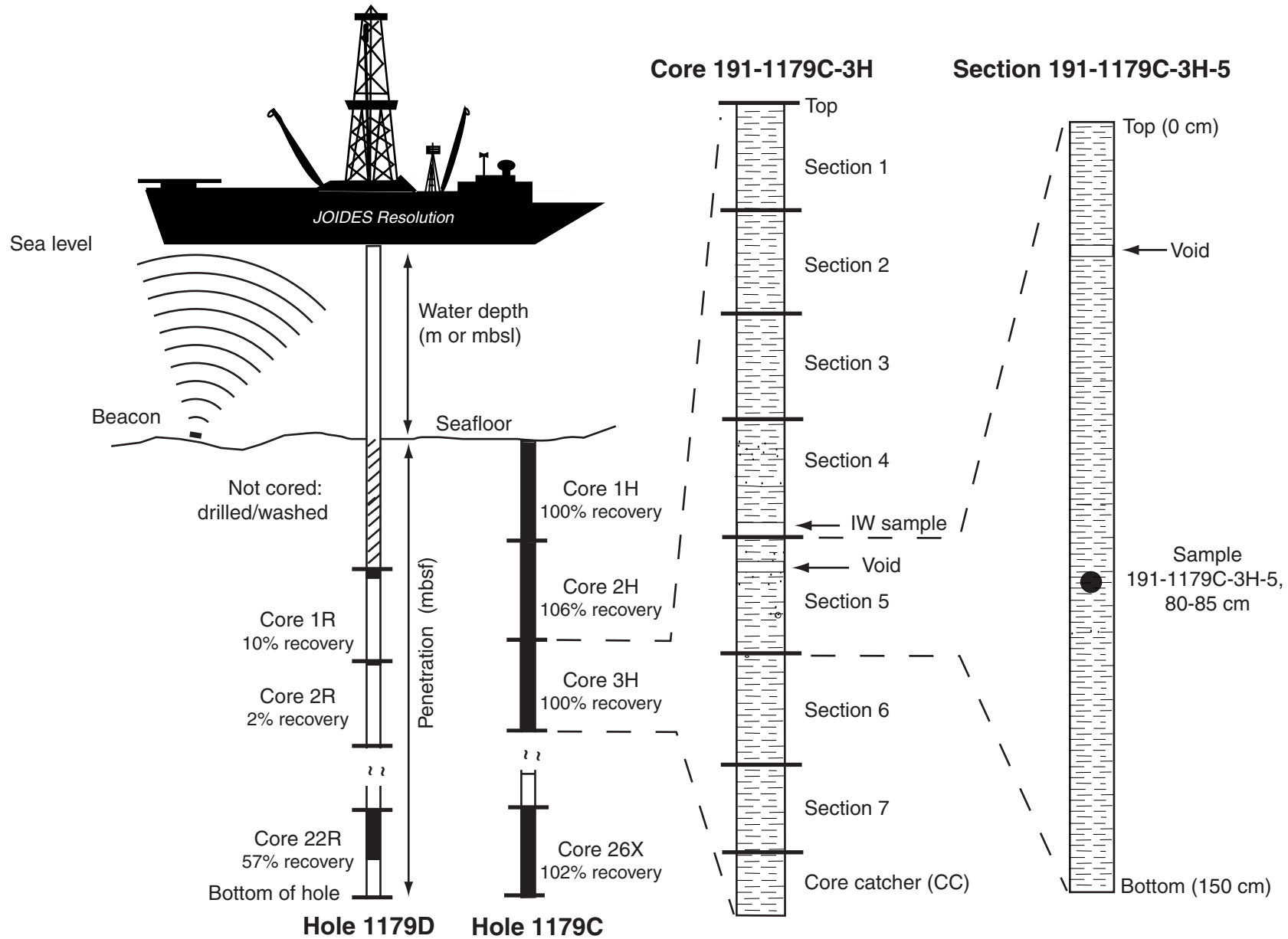


Figure F2. Key to symbols used to represent lithology, drilling disturbance, and sedimentary structures in the barrel sheets.

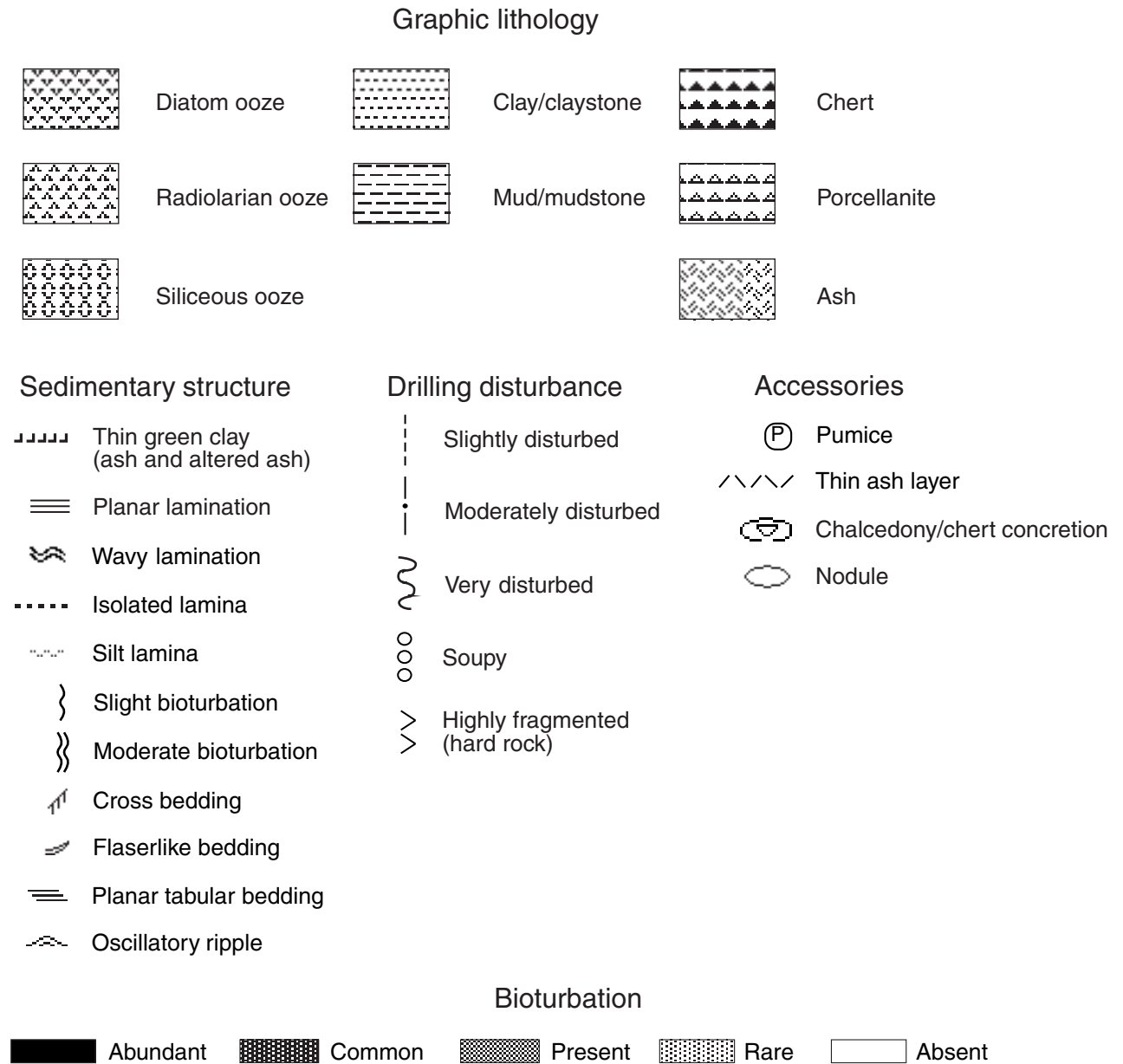


Figure F3. Nomenclature and classification of sediments used during Leg 191 and a schematic for naming mixtures of detrital, carbonate, and siliceous sediments. The inset scheme shows examples for the different principal names; modifiers in the large figure can be replaced by any valid textural or microfossil name.

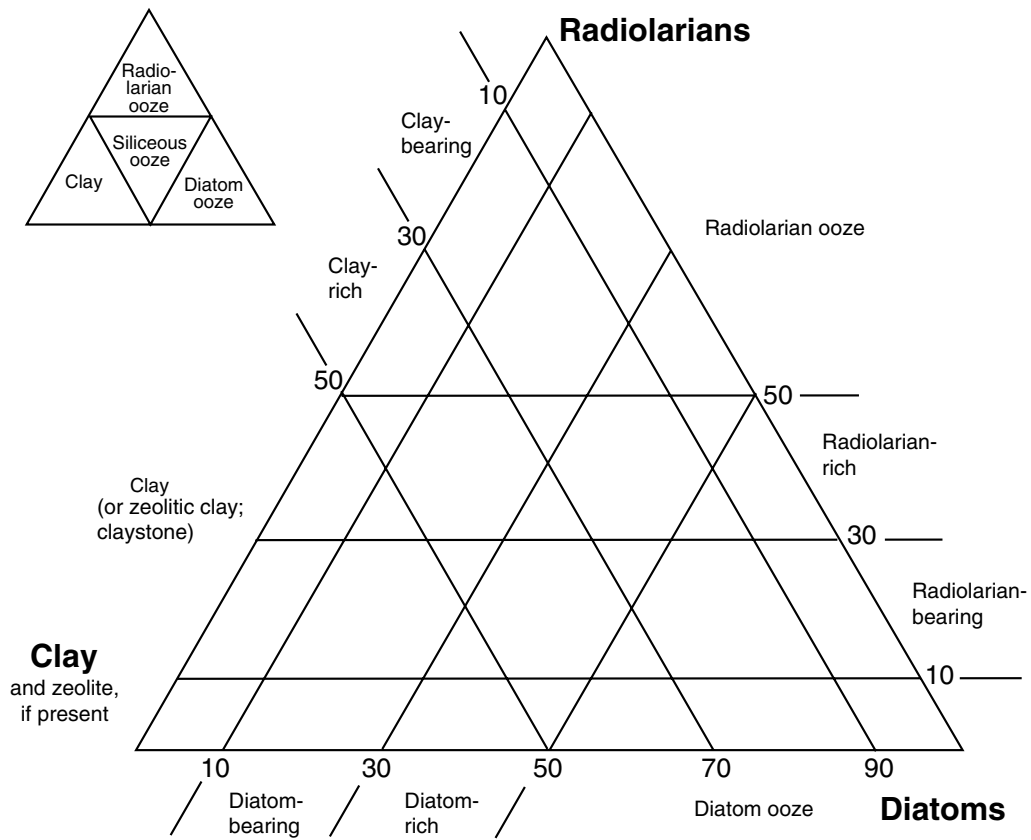


Figure F4. A sample igneous rock visual core description sheet.

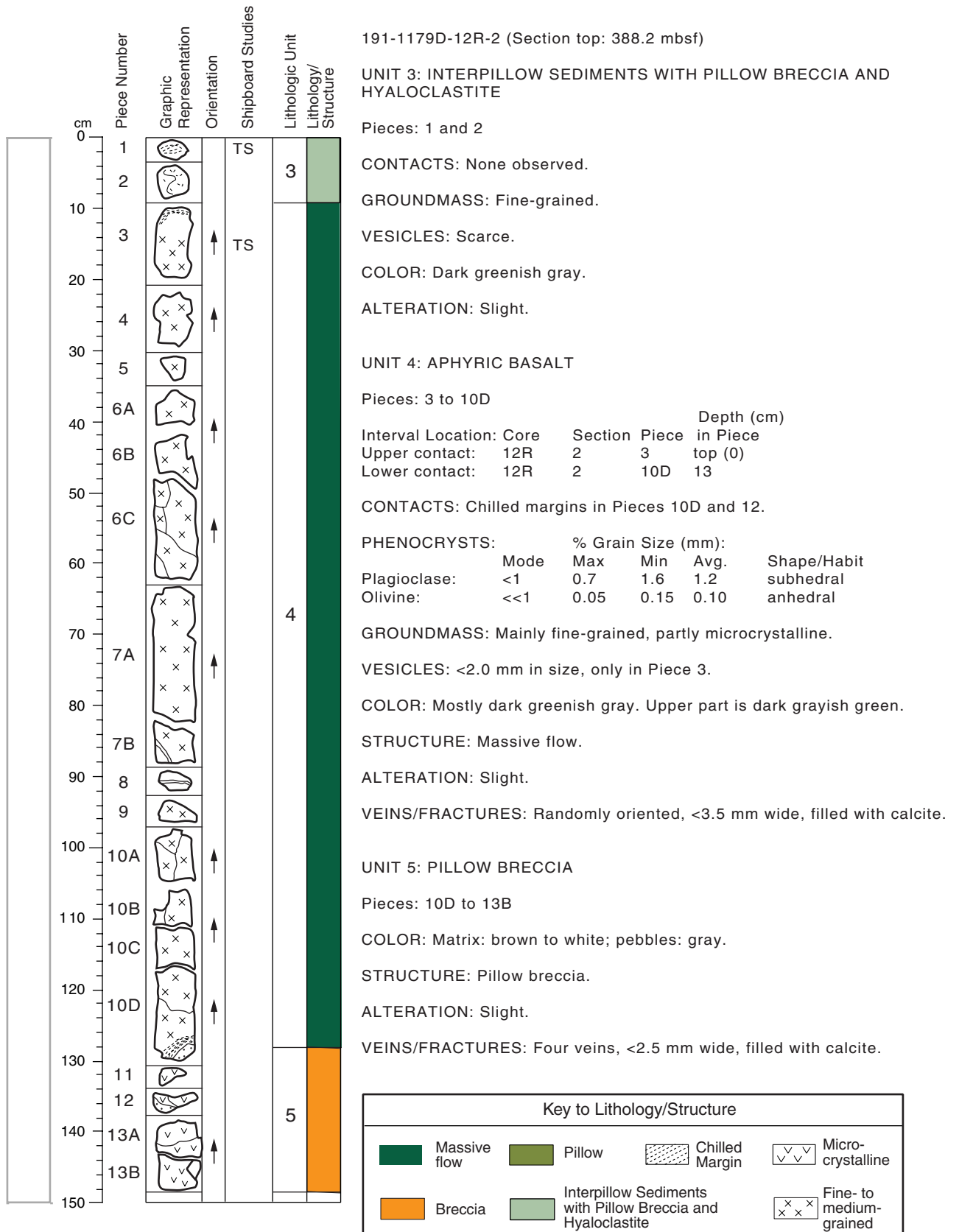


Figure F5. Coordinate systems of ODP cores and discrete paleomagnetic samples. **A.** The coordinate systems of archive- (bottom) and working-half (top) cores for paleomagnetic measurement. **B.** Orientation of discrete samples. Note that the double line (used as the reference mark for the tensor orientation tool) is on the bottom of the working half (and defines the +x-axis).

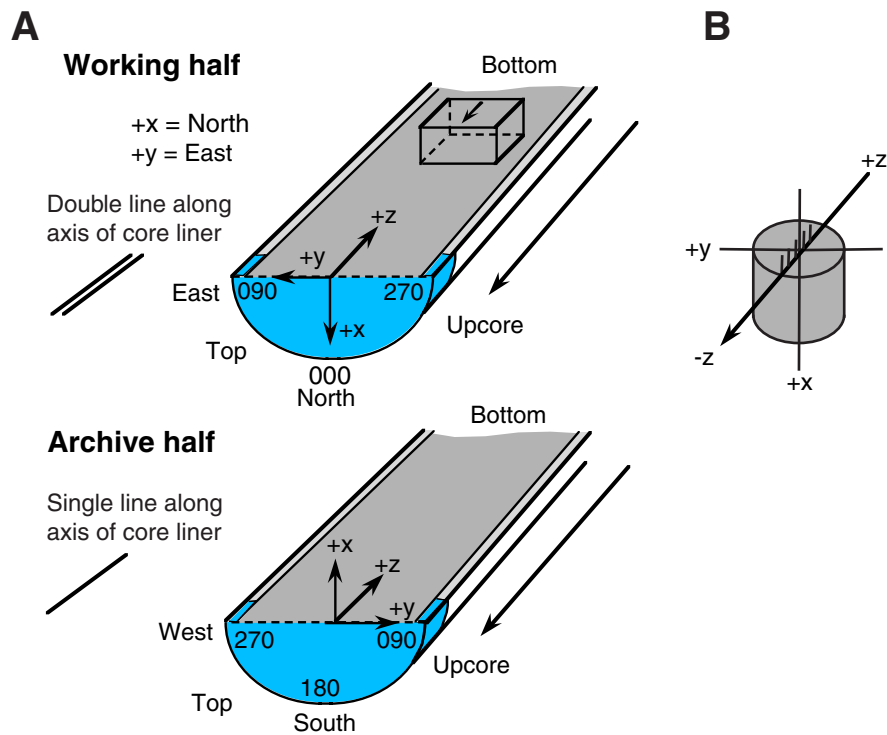


Figure F6. Miocene to Holocene geomagnetic polarity time scale (GPTS). In the polarity column, black = normal and white = reversed polarity. Absolute ages, geologic periods, and magnetic chron terminology are shown at left. This figure is based on the Berggren et al. (1995b) and Cande and Kent (1995) GPTS.

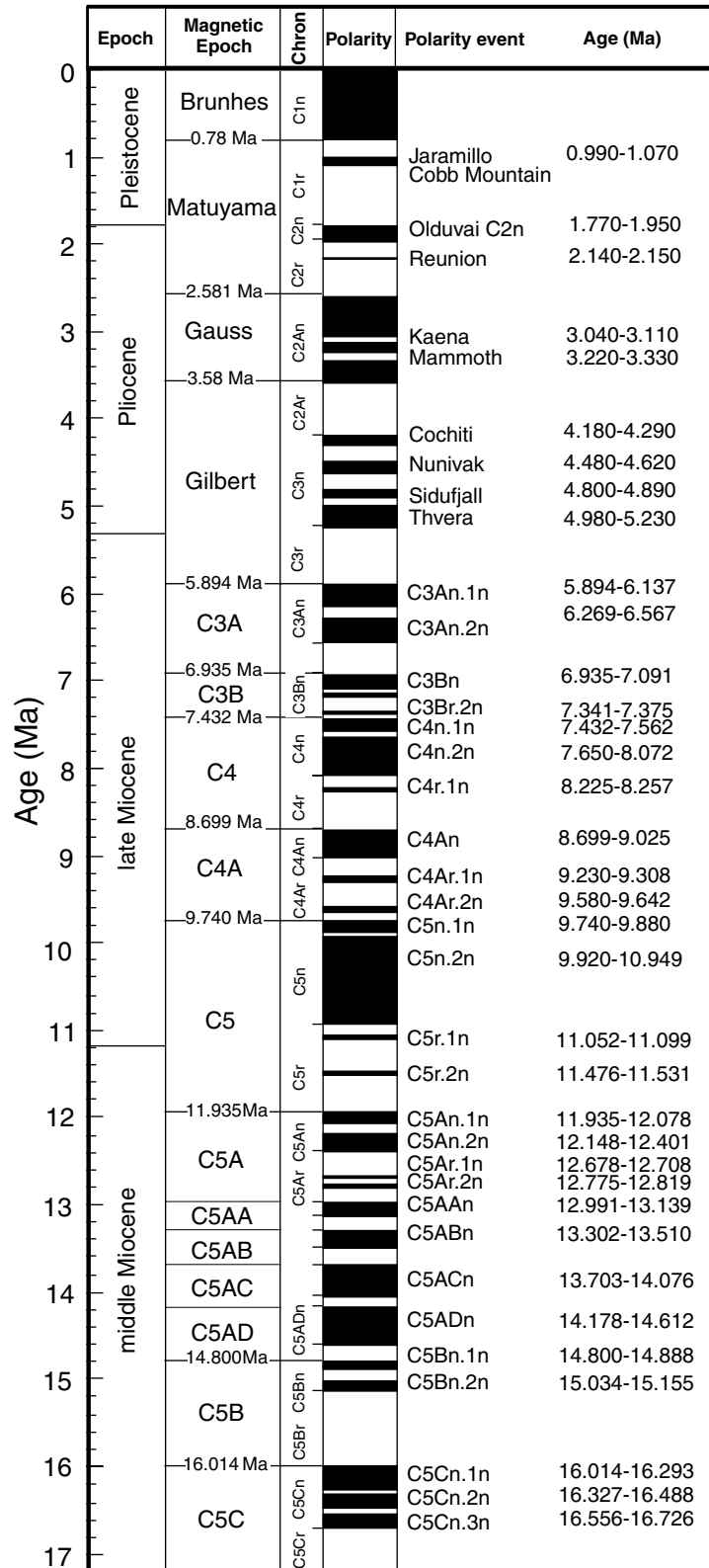


Figure F7. The triple-combination tool string. MGT = multisensor gamma-ray tool, HNGS = hostile environment natural gamma-ray sonde, APS = acceleration porosity sonde, HLDT = high-temperature lithodensity logging tool, DIT = dual induction tool, TAP = LDEO temperature, acceleration, and pressure tool.

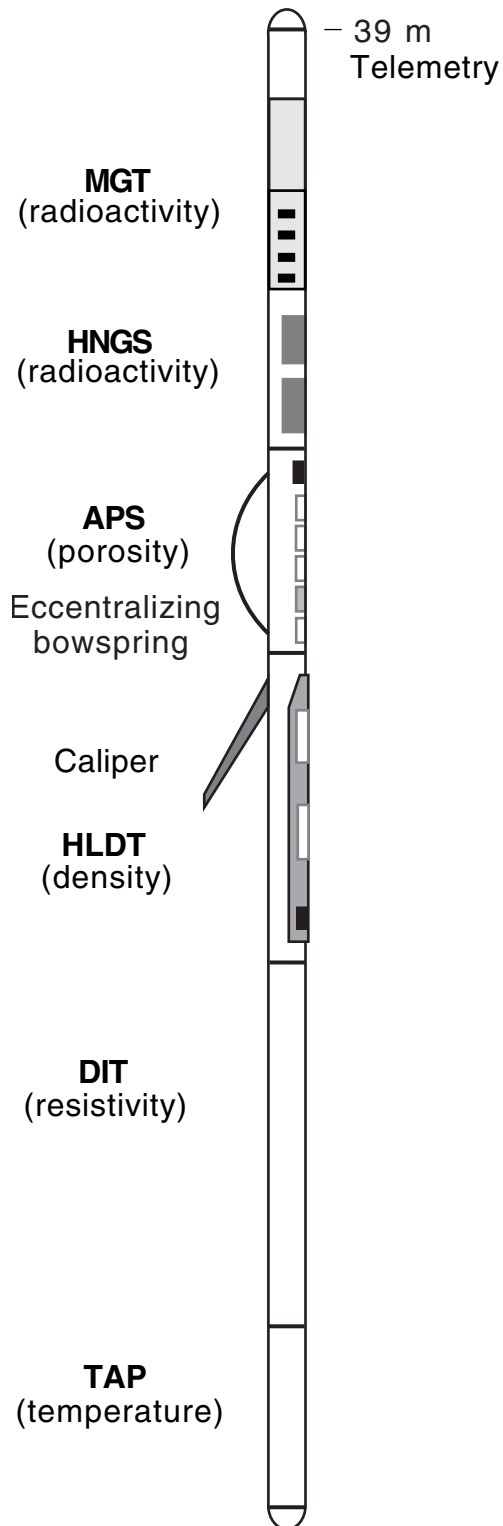


Figure F8. Schematic diagram of the multisensor gamma-ray tool.

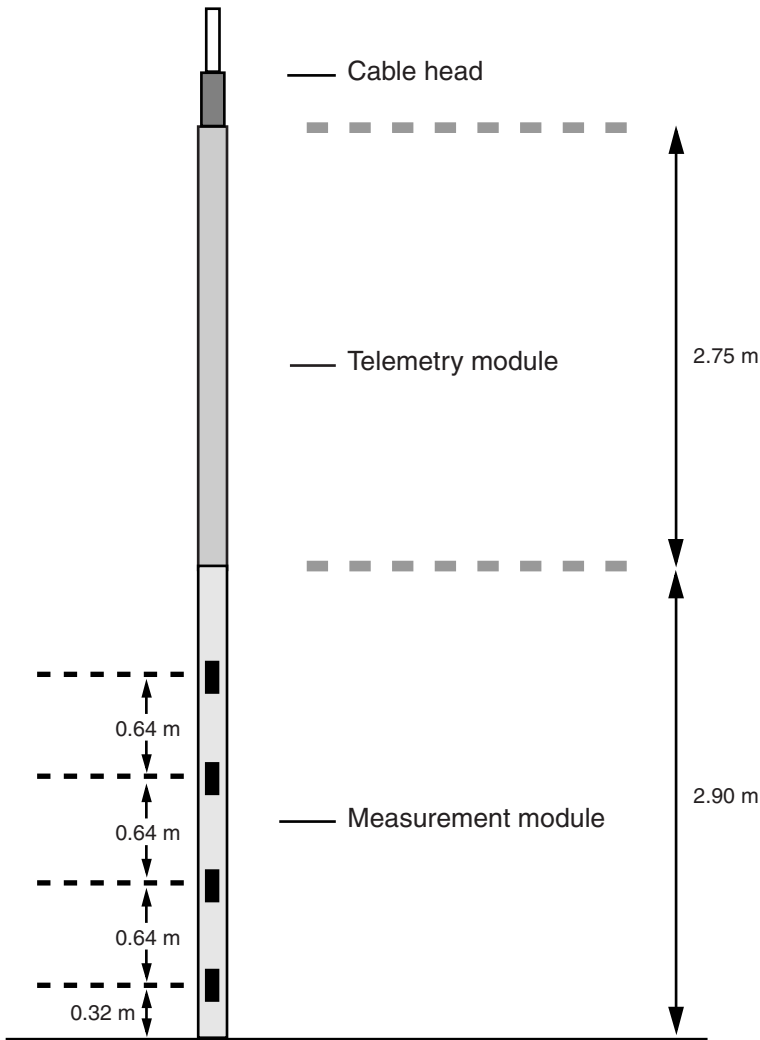


Table T1. Instrumental conditions and analytical precision for Leg 191 XRF analyses.

Element	Line	Anode	Filter	Crystal	Detector	Colimator	Peak angle (°2θ)	Background angle (°2θ)		Count time (s)		Lower limit of detection	Accuracy of calibration line	Analytical precision (1σ)
								Positive	Negative	Peak	Background			
SiO ₂	Kα	Rh	Out	PET	FPC	Standard	109.040	111.850	106.200	20	4	0.0082	0.186	0.140
TiO ₂	Kα	Rh	Out	LiF(200)	FPC	Standard	86.126	87.980	84.460	20	10	0.0008	0.012	0.003
Al ₂ O ₃	Kα	Rh	Out	PET	FPC	Standard	144.730	147.550	140.600	20	10	0.0036	0.065	0.041
Fe ₂ O ₃ *	Kα	Rh	Out	LiF(200)	Sc	Standard	57.523	58.880	56.000	10	4	0.0008	0.092	0.031
MnO	Kα	Rh	Out	LiF(200)	Sc	Standard	62.969	63.720	61.580	20	10	0.0006	0.001	0.001
MgO	Kα	Rh	Out	TAP	FPC	Standard	45.220	46.950		40	20	0.0060	0.055	0.039
CaO	Kα	Rh	Out	LiF(200)	FPC	Standard	113.067	115.250	110.550	10	4	0.0012	0.024	0.035
Na ₂ O	Kα	Rh	Out	TAP	FPC	Standard	55.171	56.800		60	20	0.0068	0.038	0.038
K ₂ O	Kα	Rh	Out	LiF(200)	FPC	Standard	136.603	139.200	133.700	10	4	0.0006	0.026	0.006
P ₂ O ₅	Kα	Rh	Out	Ge	FPC	Standard	141.070	143.250	138.100	40	20	0.0008	0.004	0.002
Sc	Kα	W	Out	LiF(200)	FPC	Standard	97.730		97.100	150	150	0.87	0.91	1.23
V	Kα	W	Out	LiF(200)	Sc	Fine	76.915		75.960	90	30	2.34	2.65	2.39
Cr	Kα	W	Out	LiF(200)	Sc	Fine	69.335	70.370	68.640	40	20	1.76	1.99	1.53
Ni	Kα	W	Out	LiF(200)	Sc	Fine	48.660	49.700	48.100	15	10	0.97	1.86	0.72
Cu	Kα	Rh	Fe	LiF(200)	Sc	Standard	45.010	45.510	44.500	20	20	1.40	3.64	2.36
Zn	Kα	W	Out	LiF(200)	Sc	Fine	41.790	42.100		20	15	0.91	2.01	1.43
Ga	Kα	Rh	Fe	LiF(200)	Sc	Standard	38.900	39.440		30	30	0.81	0.60	1.19
Rb	Kα	Rh	Cu	LiF(200)	Sc	Standard	26.600	27.120	25.760	20	20	0.65	1.64	0.68
Sr	Kα	Rh	Fe	LiF(200)	Sc	Standard	25.140	25.720	24.590	10	10	1.04	3.18	2.46
Y	Kα	Rh	Fe	LiF(200)	Sc	Standard	23.770	24.480	23.020	20	20	0.77	0.84	0.71
Zr	Kα	Rh	Fe	LiF(200)	Sc	Fine	22.540	23.020		10	10	1.13	1.66	1.74
Nb	Kα	Rh	Fe	LiF(200)	Sc	Fine	21.390	21.730		15	15	0.93	1.54	0.72
Cs	Lα	Rh	Out	LiF(200)	FPC	Fine	91.840	93.000	90.000	400	400	1.25	0.85	0.50
Ba	Lα	W	Out	LiF(200)	Sc	Standard	87.135	88.160		200	200	3.01	9.15	8.55
La	Lα	W	Out	LiF(200)	Sc	Standard	82.890	83.960	82.120	600	600	1.54	1.09	0.90
Ce	Lβ1	W	Out	LiF(200)	Sc	Fine	71.640	72.700	70.900	500	500	1.70	1.83	0.79
Nd	Lα	W	Out	LiF(200)	Sc	Standard	72.120	72.700		500	500	0.96	0.64	0.62
Sm	Lα	W	Out	LiF(200)	Sc	Standard	66.210	67.050	65.650	500	500	0.65	0.76	0.62
Gd	Lα	W	Out	LiF(200)	Sc	Fine	61.080	61.320	60.510	500	500	0.69	0.50	0.29
Dy	Lβ1	W	Ti	LiF(200)	Sc	Fine	50.290	50.470	50.050	600	600	1.04	0.55	0.89
Er	Lβ1	W	Ti	LiF(200)	Sc	Fine	46.440	46.770	46.100	600	600	1.10	0.47	0.37
Yb	Lα	Rh	Ti	LiF(200)	Sc	Fine	49.055	49.760	47.920	600	600	0.64	0.66	0.44
Hf	Lα	Rh	Ti	LiF(200)	Sc	Standard	45.880	46.150		500	500	0.49	0.39	0.63
Pb	Lβ1	Rh	Cu	LiF(200)	Sc	Standard	28.250	28.640	27.980	150	150	0.61	0.76	0.42
Th	Lα	Rh	Cu	LiF(200)	Sc	Fine	27.460	28.000	27.200	100	100	0.55	0.81	0.65

Note: * = Total Fe as Fe₂O₃. FPC = gas flow proportional counter using PR gas. Sc = naI scintillation counter. All elements were analyzed at generator settings of 50 kV and 50 mA. The lower limit of detection, accuracy of calibration, and analytical precision are shown in weight percent for major elements and in parts per million for trace elements. Analytical precision is shown as standard deviations of 10 repeated analyses of the Geological Survey of Japan reference standard JG-2 for rare earth elements and JB-1a for the others.

Table T2. Triple-combination tool measurement acronyms and units of measurement.

Tool	Output	Explanation	Units
MGT		Multisensor gamma-ray tool	
	SGR	Standard total gamma ray	gAPI
	POTA	Potassium	%
	THOR	Thorium	ppm
	URAN	Uranium	ppm
HNGS		Raw window counts and stacked spectral data	cps
		Hostile environment natural gamma-ray sonde	
	HSGR	Standard (total) gamma ray	gAPI
	HCGR	Computed gamma ray (= HSGR – uranium)	gAPI
	HFK	Formation potassium	Fractional %
	HTHO	Thorium	ppm
APS	HURA	Uranium	ppm
		Accelerator porosity sonde	
	APLC	Near array porosity (limestone corrected)	Fraction
	FPLC	Far array porosity (limestone corrected)	Fraction
	SIGF	Neutron capture cross section of the formation (Sf)	cu
HLDT	STOF	Tool standoff (computed distance from borehole wall)	in
		High-temperature lithodensity tool	
	RHOM	Bulk density (corrected)	g/cm ³
	PEFL	Photoelectric effect	barn/e ⁻
	LCAL	Caliper (measure of borehole diameter)	in
DIT	DRH	Bulk density correction	g/cm ³
		Dual induction tool	
	SFR	Spherically focused resistivity	
TAP	IDPH	Deep induction phasor-processed resistivity	Ωm
	IMPH	Medium induction phasor-processed resistivity	Ωm
	SFLU	Shallow spherically focused resistivity	Ωm
		High-resolution temperature/acceleration/pressure tool	°C, m/s ² , psi

Table T3. Principal channels of the triple-combination tool.

Individual tools	Properties measured	Sample interval (cm)	Approximate vertical resolution (cm)	Approximate depth of investigation (cm)
HNGS	Natural gamma ray	15	45	Variable
APS	Porosity	5 and 15	30	15
HLDT	Bulk density, PEF	15	38	15
DIT-SFL	Resistivity	15	150/90/60	150/76/38
TAP	Temperature	1/s	NA	NA
	Tool acceleration	4/s	NA	NA
	Pressure	1/s	NA	NA

Notes: See Table T2, p. 47, for explanations of acronyms. NA = not applicable, PEF = photoelectric effect.

CHAPTER NOTE*

- N1. 24 August 2001—Errata: After this chapter was published, it was found that the World Wide Web addresses in the Blum, 1997, and Gieskes et al., 1991, references contained errors. The correct Web addresses appear in this version.